The Theory, Manufacture, Structure and Performance of N.P.L. X-Ray Gratings

A. Franks, K. Lindsey, J. M. Bennett, R. J. Speer, D. Turner and D. J. Hunt

Email alerting service	Receive free email alerts when new articles cite this article - sign up in the box at the top right-hand corner of the article or click **here**

[503]

THE THEORY, MANUFACTURE, STRUCTURE AND PERFORMANCE OF N.P.L. X-RAY GRATINGS

By A. FRANKS and K. LINDSEY

Division of Inorganic and Metallic Structure, National Physical Laboratory, Teddington, Middlesex

J. M. BENNETT,† R. J. SPEER and D. TURNER

Department of Physics, Imperial College of Science and Technology, Prince Consort Road, London S.W. 7

and D. J. HUNT

Atomic Weapons Research Establishment, Aldermaston, Berkshire

[Plates 16–19]

CONTENTS

† Present address: Rank Xerox Development Laboratory, Welwyn Garden City.

X-ray gratings have been developed for use in the wavelength region of 0.01–20 nm, where it is required to employ a grazing incidence configuration. The gratings have a rectangular profile and radiation is diffracted both from the tops and bottoms of the grooves. They therefore differ from blazed gratings, used at grazing incidence, in that a substantial portion of the grating participates in the diffraction process.

A scalar diffraction theory has been developed which demonstrates that grating diffraction efficiency varies periodically with wavelength, pitch, groove depth and incidence angle. The theory can be used to optimize grating parameters for most efficient use in any selected region of the spectrum.

The gratings are produced by processing a ruled 300 lines per millimetre master grating, so that surface profile defects introduced by ruling are eliminated.

Grating performance has been assessed by means of a specially designed grating analyser in addition to spectrometers and a spectrograph. The experimental results are in qualitative agreement with theory. At very short wavelengths of 0.05 nm and grazing incidence angles of about 5′, the diffraction efficiency in the first order is below 1 %. The efficiency rises rapidly to between 5 and 10 % at 0.15 nm and to 20 % in the 1 nm region where the incidence angles are typically a few degrees.

1. INTRODUCTION

During the past decade, there has been an upsurge of interest in X-ray and ultraviolet spectroscopy in the wavelength region of 0.01–50 nm. This spectral region is important, for example, in analysis of elements and compounds by the electron microprobe or by X-ray fluorescence, in the study of extra-terrestrial radiation and in the analysis of radiation emitted by plasmas, as well as in the study of classical emission and absorption processes.

In the range 50–10 nm, diffraction gratings are the sole means of dispersing radiation, while shorter wavelengths may be dispersed by gratings, crystals or pseudo-crystals. Pseudo-crystals are produced by successive deposition of monolayers of metals salts of straight chained fatty acids (Blodgett 1935). The spacing between successive layers is, typically, 5 nm, so that the maximum wavelength which can be dispersed is 10 nm. The range over which they are used normally extends from 10 nm down to 2 nm. A wide variety of natural or synthetic crystals is employed to disperse radiation below 2 nm.

A basic difference between grating and crystal diffraction is, that for the latter, the condition imposed by Bragg's law demands that diffraction of a particular wavelength can take place

only at a specific angle of incidence and this difference can confer advantages to grating spectroscopy which are worth noting.

In the case of crystal diffraction, a focused spectrum of a stationary point source can be obtained only by means of a scanning mechanism (it is possible to obtain spectra over a limited region if the source is extended, or if the crystal is suitably curved, usually in a convex form, so that small sections of the crystal are oriented to diffract over a limited wavelength range). On the other hand, for grating diffraction, a complete focused spectrum can be recorded at a single incidence setting. This property of the grating enables spectroscopy to be carried out with the aid of simple spectrographs which require no moving parts. In crystal spectrometers, the motion of the crystal and detector must be linked to enable the detector to rotate at twice the rate of crystal. This additional complexity is however partially off-set by the requirement that the grating spectrometer must be constructed to finer limits, since, in general, incidence and diffraction angles are quite small. The small numerical aperture of grating spectrometers may also make source alinement more tedious.

The advantage of simultaneous recording of a complete spectrum as opposed to sequential recording is particularly marked in studying weak sources or where the recording time is limited by some external factor (e.g. a rocket flight-time). A further example of the latter occurs in thermonuclear fusion research where the spectrum of the plasma may appear for characteristic times of the order of a microsecond only. Spectra may be recorded photographically or by the use of suitably positioned fast solid state detectors and may be time-resolved at several wavelengths simultaneously.

In the 2–10 nm region, gratings have an additional advantage in that their intrinsic resolving power may be one or two orders of magnitude greater than that of pseudo-crystals. The theoretical resolving power is equal to the number of effective diffracting elements which, for the pseudo-crystal, varies between 50 and 150, and is limited by absorption of the soft X-radiation within the crystal. However, the practical resolving power of a grating is very dependent on the mechanical tolerances, particularly the entrance slit width, of the associated spectrometer or spectrograph and probably, in general, the gain in resolution is in the region of one order of magnitude only. A further disadvantage of pseudo-crystals is that the diffracted beam is often accompanied by background produced by the specular reflexion of long wavelength X-rays, which coincides in direction with the diffracted beam.

There is ample evidence (Speer 1972) that the current commercially available diffraction gratings are inefficient in the X-ray region of the spectrum. Nearly all such gratings are designed to have a shallow blaze sawtooth profile and when the grazing incidence angles do not appreciably exceed the critical angle for total external reflexion, only the uppermost tip of this profile is illuminated (incidence angles may vary between 5′ for radiation of wavelength 0.05 nm to 4° for radiation of 5 nm). This region of the profile which typically is 30 nm high, even though inverted through replication, cannot be controlled to this scale in the diamond ruling process and this is the most probable reason for the wide variability between such rulings – even of identical specifications. In figure 1, the performance data is given on the best 15 blazed gratings out of 50 examined to date at the grating research laboratory at Imperial College.

The ratio of the first order diffracted to incident intensity is plotted as a function of grazing angle and the results are also classified in terms of groove spacing. The monotonic decline with ruling frequency for this shallow blazed type ruling is interpreted as due to a progressive loss of control over the shape of the diffracting element. As the grating spacing increases, it would

be expected that the diffraction efficiency would tend towards the product of the reflexion coefficient and area illuminated, while for decreasing grating spacing, the incoherent scattering would increase at the expense of diffraction efficiency, the latter tending to zero.

An alternative type of X-ray grating, described in detail below, consists of optically flat or curved surfaces interrupted by grooves which may also participate in the diffraction process. Important advantages are that a much larger proportion of the surface contributes to the diffraction and that the quality of the surface is under control. Early developments of these gratings were described by Sayce & Franks (1964): these gratings are termed N.P.L. X-ray gratings.
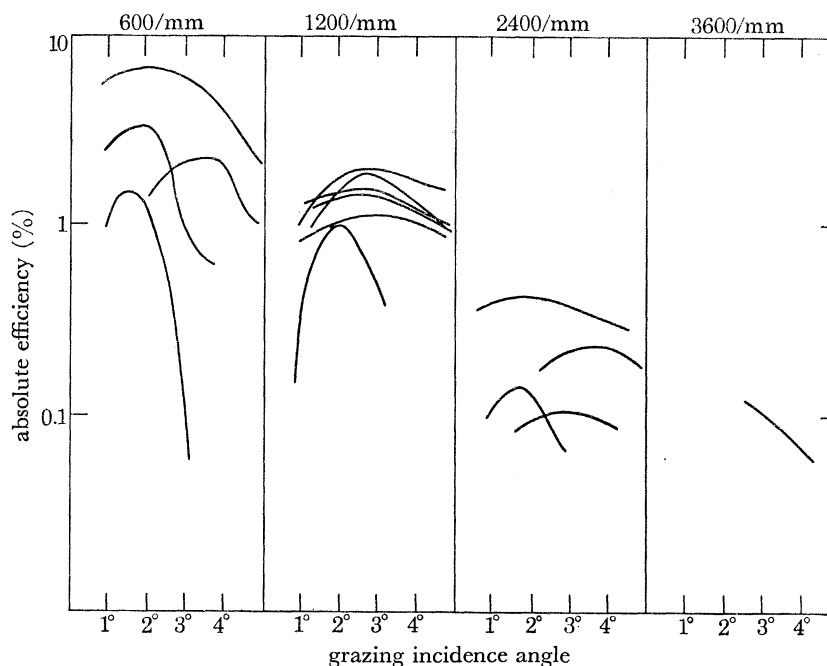

FIGURE 1. Variation of absolute diffraction efficiency in the first order as a function of incidence angle for blazed gratings of different spacings, at wavelengths of 0.84, 2.3 and 4.4 nm.

The further development of these gratings, particularly of the phase grating, in which X-rays are diffracted from both the top and bottom of the groove, required a study to be made of the factors which decrease reflectivity. There are three important classes of surface defect which have been found to affect grating performance adversely and these must be eliminated or reduced as much as possible to enable the grating to diffract efficiently.

Gross imperfections fall in the first class of defects. These include burrs and other ruling tool detritus. The techniques employed in X-ray grating manufacture were devised to avoid the formation of these defects.

Microscopic imperfections which are several times larger than X-ray wavelengths form the second class of defects. It is easy to show that a bump or depression of height H on the grating surface will introduce a path difference between the beams reflected from the imperfection and the surface of $2H\sin i$, where i is the glancing angle of incidence. If this path difference were equal to $\frac{1}{2}\lambda$, the rays would interfere destructively and the energy would manifest itself outside the geometrical reflexion direction. In this case,

$$2H\sin i = \tfrac{1}{2}\lambda \quad \text{or} \quad H = \tfrac{1}{4}\lambda/i \quad \text{since } i \text{ is small.}$$
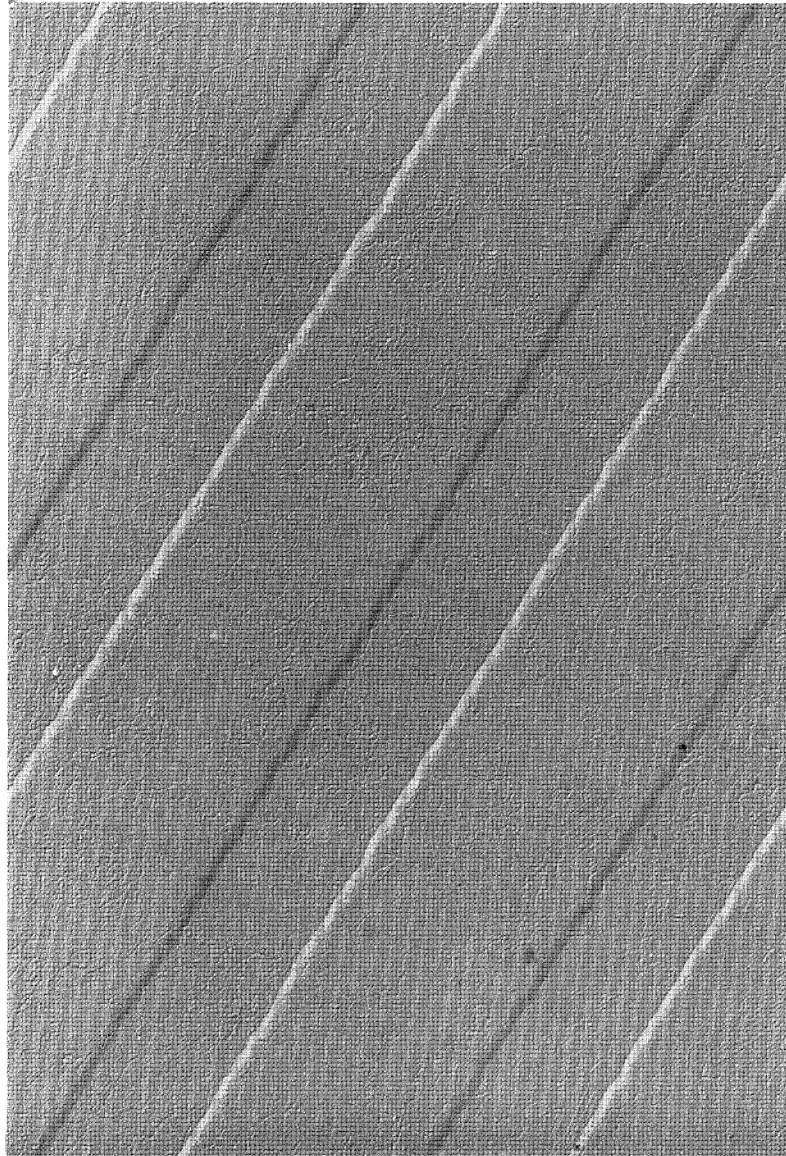
FIGURE 2. Electron micrograph of N.P.L. X-ray phase grating (300 lines/mm) illustrating the laminar configuration (the fine surface structure is produced by the electron microscope replica technique employed).

The smaller the value of i, the larger may be the value of H before destructive interference occurs. Now the largest value of i at which total reflexion takes place is roughly proportional to λ and λ/i is therefore approximately constant. Substituting this constant in the equation yields a value of H, for which destructive interference takes place, of between 10 and 20 nm. The surface roughness should therefore be at least one-fifth of this, between 2 and 4 nm, but the smaller the better. It will be shown later that phase gratings may have groove depths of this order of magnitude and larger and it is therefore important that if any such defects exist, that they should be small in number and in lateral extent.

The diffraction, as opposed to the reflexion, condition is even more stringent. The height of the imperfection for which destructive interference occurs is $\frac{1}{2}\lambda(i+\theta)$, where θ is the diffraction angle. It will be shown in §6(c)(ii) that the reduction in diffraction efficiency at wavelengths below 0.1 nm may, in the main, be attributed to this factor.

The third class of defects are undulations of very small slope. These result directly from the geometry and the motions employed in lapping and polishing the grating blank. They usually cover the surface completely and cause a large proportion of the incident illumination to be spread about the centrally reflected and diffracted beams. Only by careful control of the production process can the spread be reduced to about one or two arc secs, which is not significant for most grating applications. The effect of this type of defect is discussed in §5(a).

2. GENERAL DESCRIPTION

Unlike the gratings described previously, all the gratings referred to in this paper have a laminar structure as shown in figure 2, plate 16, and in profile in figure 16. In this type of grating, beams can be diffracted from both the tops and bottoms of the grooves and, if conditions are chosen correctly, the path difference of the totally reflected or zero order beams can be made such that they interfere with each other destructively, so that more of the energy, usually lost in reflexion, is transferred into the diffracted beams. The properties of these phase gratings are in one sense intermediate between the conventional blazed grating and a simple grating consisting of a flat surface interrupted by grooves. The theoretical maximum diffraction efficiency in the first order of the latter grating is about 10 % assuming that surface is 100 % reflecting, while that of a blazed grating at normal incidence is 100 %. The diffraction efficiency calculated on the basis of a 100 % reflexion efficiency is termed the geometrical diffraction efficiency. This figure is nowhere near achieved in practice, as we have seen, because of the difficulties in making a sufficiently smooth and precise saw tooth form and because of shadowing effects at grazing incidence.

Three types of phase gratings (figure 3) are envisaged; (a) unmasked, where the whole grating is fully effective, (b) partially masked, where part of the groove is in the shadow cast by the upper surface – the land – and (c) fully masked, where still less of the groove is effective, because the diffracted rays are absorbed by the step at the leading edge of the groove. In the latter case we can assume, for simplicity, that the beam is totally absorbed by the material of the grating. Under normal incidence conditions, the unmasked type would have a first order geometrical diffraction efficiency of 40 % but this is an unattainable ideal. In practice, conditions hold which lie somewhere between the extremes of unmasked and fully masked. For instance, with soft, easily absorbed radiation and relatively large groove depths, a performance approaching that of the fully masked condition may be achieved, while with harder radiation

the unmasked condition is approached. By suitable choice of parameters it is possible for the geometrical diffraction efficiencies to exceed 30 %. At short wavelengths and small incidence angles, where the radiation can penetrate the material supporting the land, the next or subsequent grooves may be illuminated thus giving rise to phase grating behaviour although the grooves may be completely in the shadow of the contiguous lands.
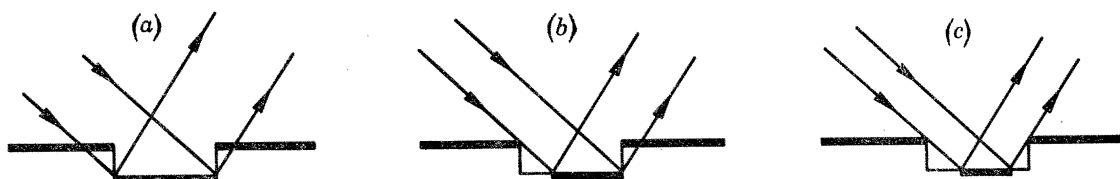

FIGURE 3. Phase gratings. (a) Unmasked, (b) partially masked, (c) fully masked. The effective parts of the grating are indicated by heavy lines.

3. THE THEORY OF PHASE GRATINGS

The idealized profile of an N.P.L. phase grating is shown in figure 4. If the groove depth is h, it is clear that destructive interference would occur in the reflected beam at a wavelength $\lambda = 4h$, at normal incidence. The energy in the incident beam is thus redistributed among the diffracted beams to enhance the diffraction efficiency.
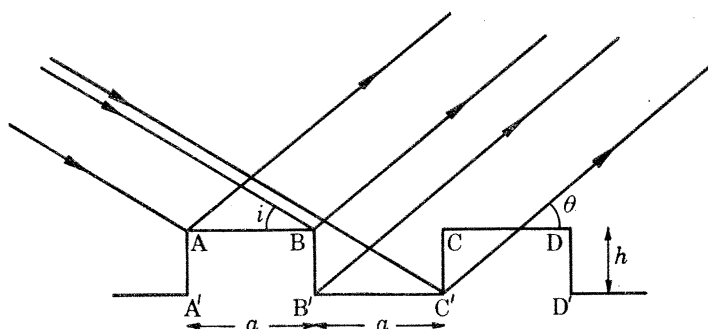

FIGURE 4. Idealized profile of phase grating. The land width AB equals the groove width B'C'. Grazing angles of incidence and diffraction are i and θ respectively.

The theoretical treatment of phase gratings in this paper follows that of Hellwege (1937), except that it is modified to take into account the small angles of grazing incidence which are necessarily used in the X-ray region of the spectrum.

The only case which shall be considered in detail is illustrated in figure 4 where the land width AB is equal to the groove width B'C'. This simplifies the algebra and also approximates quite closely to the configuration of a practical X-ray grating.

The grating constant $d = 2a$ and the groove depth AA' $= h$, the grazing angles of incidence and diffraction are denoted by i and θ respectively.

In Hellwege's treatment, it is assumed that the whole of the diffracting areas AB, $B'C'$, ..., etc., are completely illuminated by the incident radiation; this is a good approximation for near normal incidence where the shadows of the land areas cast on the grooves are small. If we assume this initially and also that the grating absorbs none of the incident radiation and that

the reflexion coefficient is 100%, then following Hellwege, the absolute efficiency, defined as the ratio of the intensity diffracted in any odd order m and the incident intensity is

$$E_m = \frac{400}{m^2\pi^2}\sin^2\tfrac{1}{2}\delta',\tag{1}$$

where $\delta' = (2\pi/\lambda)h(\sin i + \sin\theta)$, while for the zero order the efficiency is $E_0 = 100\cos^2\tfrac{1}{2}\delta'$.

In this treatment we are primarily interested in diffraction efficiency in the first order as a function of wavelength, incident angle and groove depth.
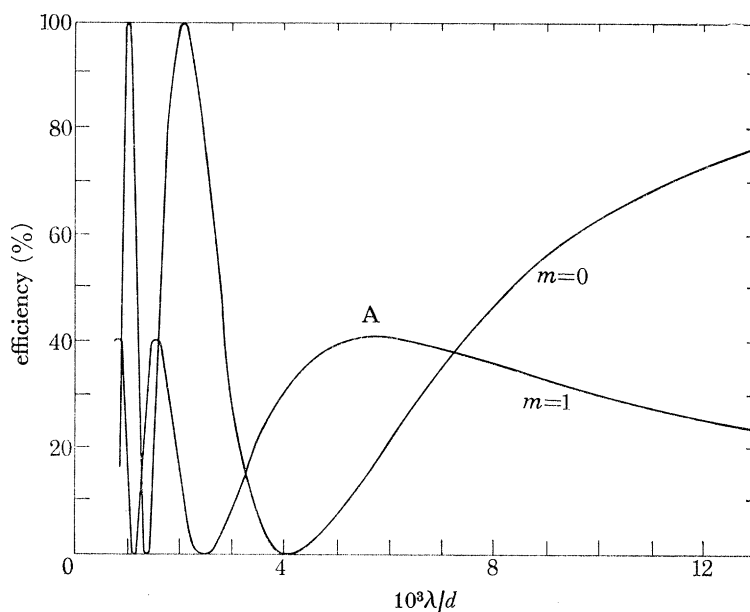

FIGURE 5. Theoretical zero and first order diffraction efficiencies as a function of wavelength, at an incidence angle of 3°, the grating pitch is d and groove depth $h = 0.01d$.

Figure 5 shows the zero and first order absolute efficiency as a function of wavelength, at a grazing angle of 3° and a groove depth of 0.01d. The oscillatory nature of the functions plotted differs from the behaviour of amplitude or blaze gratings. The maximum efficiency recorded in the first order is just over 40%, which is a fourfold increase over the theoretical maximum efficiency of an amplitude grating with a land-to-groove width ratio of unity. The first order maxima are displaced slightly with respect to the minima of the zeroth order, in the direction of increasing wavelength.

It is evident from figure 5 that the most profitable region in which to use the grating to obtain high efficiency in the first order, *over a large range of wavelengths* is that denoted by A. This will be referred to as the 'primary maximum of efficiency' in the first order.

For a given groove depth, the positions of the primary maxima in the first order for various incidence angles are shown in figure 6. The primary maximum is displaced in the direction of increasing wavelength for increasing angle. This is of practical importance because as the wavelength increases larger incidence angles may be employed, while at the same time satisfying the condition for total external reflexion (the critical angle of total external reflexion is approximately proportional to wavelength). Thus a grating of a given groove depth may be used with high efficiency over a wide range of wavelengths by varying the angle of incidence so that the

primary maximum lies in the wavelength region of interest. In situations where the angle of incidence cannot be varied, a groove depth can be selected to enable the primary maximum to coincide with the spectral region of interest. Figure 7 shows the efficiency as a function of wavelength for different groove depths and at a fixed incidence angle of 3°. Figures 5, 6 and 7 illustrate that the broadest (i.e. largest wavelength range) primary maximum exists at large values of λ/d. It would therefore seem to be advantageous to use a small grating pitch. For
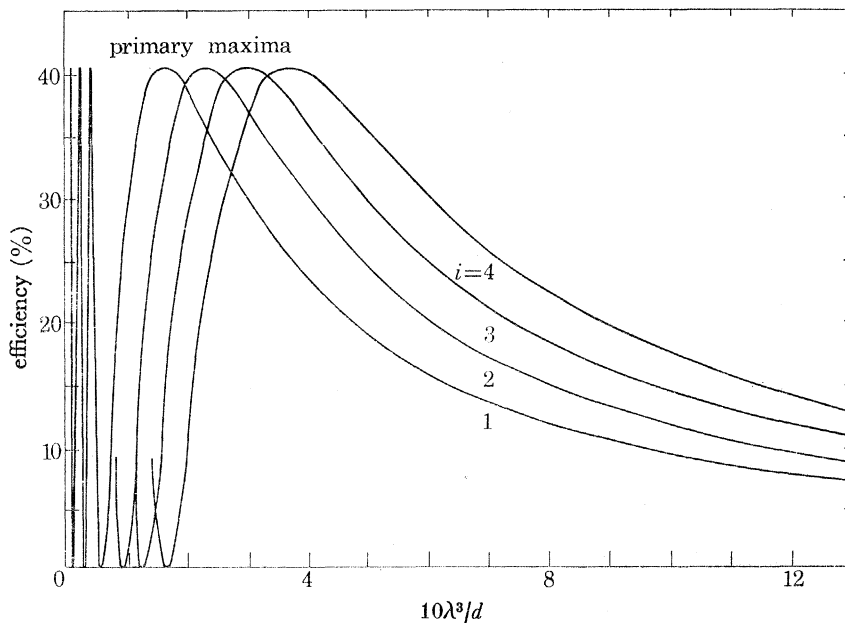
FIGURE 6. Theoretical first order diffraction efficiences as a function of wavelength for different incidence angles i and for a groove depth $h = 0.01d$.
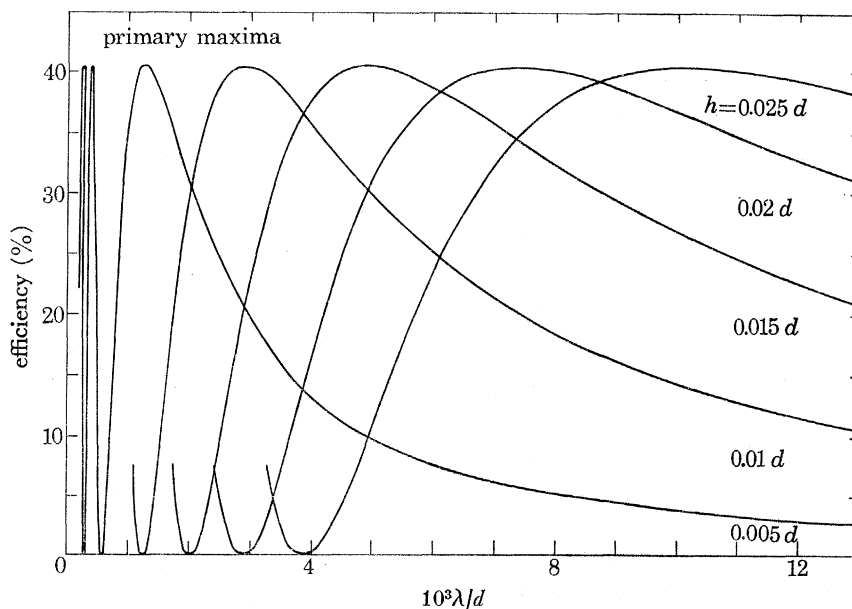
FIGURE 7. Theoretical first order diffraction efficiencies as a function of wavelength for different groove depths h at an incidence angle of 3°.

short wavelengths, shallow incidence angles must be used in order to remain within the total external reflexion condition, and from figure 6, this displaces the primary maximum in the direction of decreasing wavelength range. Shallower grooves are required for dispersion of the shorter wavelenths (figure 7) and again this condition displaces the primary maximum in the same direction. Thus it can be seen that there exists optimum values of pitch, groove depth and incidence angle for any particular wavelength. The position of the primary maximum can be obtained as a function of these three parameters by differentiation of equation (1). This yields the expression

$$\frac{\lambda}{d} = \left(2m\,\cos\,i + \frac{n\sin i}{h/d}\right) \Big/ \left(\frac{n^2}{(2h/d)^2} + m^2\right), \tag{2}$$

where $n = 1$ for the primary maximum of efficiency. In this equation, if n is odd, the stationary point on the efficiency curve is a maximum while if n is even, it is a minimum.

Manipulation of equation (2) yields the following users' equations

(a) Selection of odd order diffracted efficiency maxima proceeds first by the choice of h, from

$$\left(\frac{1}{h} - \frac{1}{h_0}\right)^2 = \left(\frac{8\cos i}{\lambda d}\right) m + \frac{1}{h_0^2},$$

where $h_0 = \frac{1}{2}\lambda/\sin i$ is a parameter determined by the experimental requirements on λ and i and represents the condition for zero order cancellation.

(b) With a chosen h, the optimum conditions can be satisfied at other wavelengths

$$\lambda = 4h\sin i + (8mh^2/d)\,\cos i.$$

(c) Alternatively we may express

$$\sin i \approx \frac{\lambda}{4h} - \frac{2mh}{d}$$

which locates the required value of i for given m, λ, h and d.

Two independent equations of great simplicity can be derived for h by rewriting equation (2) for the optimum efficiency condition at $m = \pm 1$, namely

$$h = \tfrac{1}{4}d(_{-1}i_{\mathrm{opt}} - {}_{+1}i_{\mathrm{opt}})$$

and

$$h = \lambda/[2(_{-1}i_{\mathrm{opt}} + {}_{+1}i_{\mathrm{opt}})],$$

where $_{-1}i_{\mathrm{opt}}$ and $_{+1}i_{\mathrm{opt}}$ refer to the incidence angles yielding the maximum efficiencies for the order -1 and $+1$ respectively. These equations can be used to deduce an effective value for h from the measured efficiency curves.

As discussed in §2, the groove areas are not completely illuminated because of shadowing effects. The effects of partial and full masking are shown in figure 8 for the same grating parameters as in figure 7. The general characteristics of the curves are similar in the masked and unmasked situations: the major differences being that the peak efficiencies are reduced and that in the limit, where the groove is entirely shaded, the efficiency will drop to about 10%, equal to the efficiency of the equivalent amplitude grating with equal land and groove widths, where the grooves do not contribute to the diffracted energy.

In the theory developed so far, the following assumptions have been made:

(i) that no absorption of the beam takes place at small grazing angles;

(ii) that the reflexion coefficient is 100%; and

(iii) that the diffracted beams are unpolarized.

Fresnel theory appears to be perfectly adequate (Stewardson & Underwood 1965; Parratt 1954) to account for the experimental measurements of X-ray reflectivity. By substitution in the standard equations, it can easily be shown that the maximum difference between the reflectivities of the parallel and perpendicular polarized radiations is less than 0.1 % for wavelengths of 1 nm and 0.01 % for 0.15 nm at their respective critical angles of incidence. Radiation should therefore be virtually unpolarized at small glancing angles. This has been confirmed experimentally by Speer (1966). In view of this, it is considered justifiable, at this stage, to apply scalar theory in the present investigation.
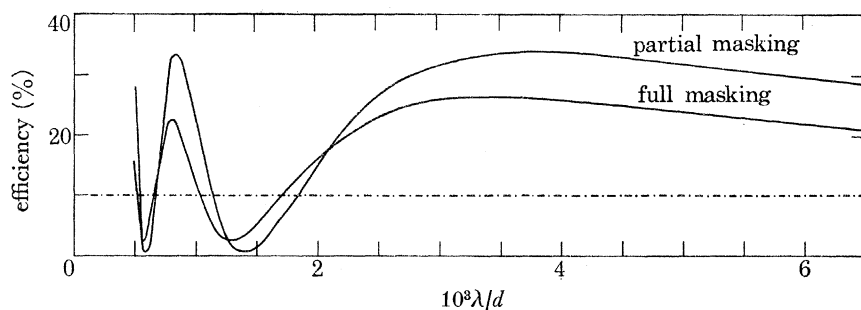

FIGURE 8. Theoretical first order diffraction efficiencies as a function of wavelength at an incidence angle of 3° and for a groove depth $h = 0.01d$, in the case of full and partial masking.

(a) Scalar model of the phase grating

Early measurements of diffraction efficiency at 4.45 nm (Franks & Lindsey 1966) and at 0.15 nm gave oscillatory results, characteristic of a phase grating, although, in the latter case, at the small incidence angles employed, less than 20', it was clear that the grooves were completely shadowed by their contiguous land areas. It is therefore suggested that the radiation penetrates the material barriers supporting the land areas, thus allowing the next or subsequent grooves to be illuminated. This consideration is built into the present model, along with the following:

(i) The absorption at the surface of the grating is taken into account by assuming that the energy available for distribution among the spectral orders is that which would be reflected from a smooth surface composed of the same material as that of the grating. The intensity diffracted from the grating surface is given by $I = RI_0$ where I_0 is the incident intensity and R the reflectivity.

(ii) The radiation which penetrates the grating material supporting the land area is partially absorbed by the material according to the relation $I = I_0 \exp(-\mu_1 x)$ where μ_1 is the linear absorption coefficient, x the distance traversed in the material, and I and I_0, the transmitted and incident intensities respectively.

(iii) Since the grating material has a refractive index different from unity, the radiation in (ii) will in general be retarded in phase by an amount given by

$$\delta_m = 2\pi(n-1)x/\lambda,$$

where n is the refractive index.

The phase change on reflexion may be ignored, because the grating surface is considered to be composed of the same material over its whole area.

The modes of operation of the model are illustrated in figure 9. Figure 9a shows the land AB and contiguous groove B'C' illuminated directly by the incident radiation. The radiation on CC' is absorbed by the grating material, this being indicated by cross-hatching. At a given angle of incidence i_s, the groove B'C' will be completely in the shadow of land AB as shown in figure 9b. In this configuration, all the radiation incident on the groove will be absorbed. The effect of a further slight reduction in i is illustrated in figure 9c where the radiation incident on BC no longer illuminates surface B'C' in that groove, but instead illuminates part of the groove
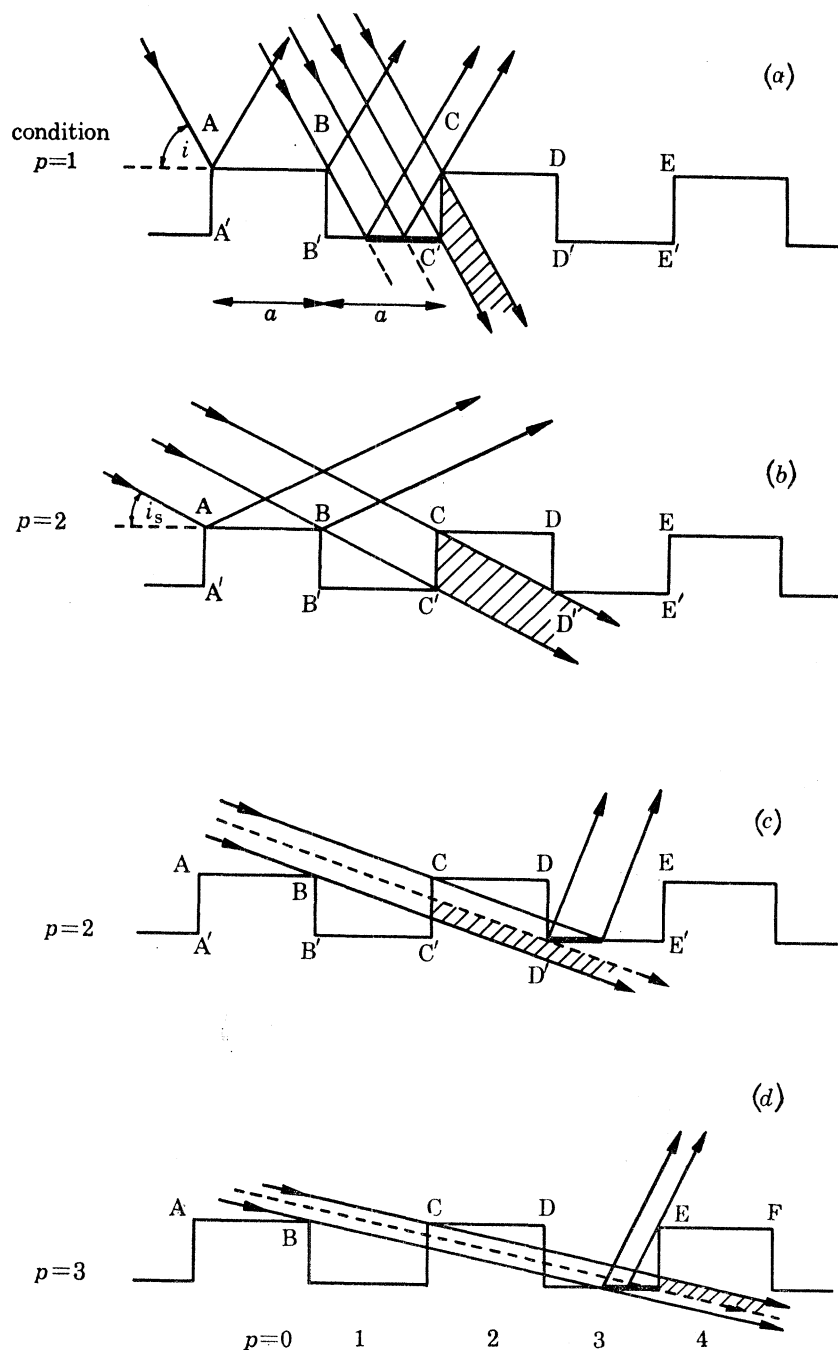

FIGURE 9. Illumination of non-contiguous grooves.

surface D'E'. To complete the sequence, figure $9d$ shows a shallower angle still, where the ray through B now passes into the groove DE and the right-hand side of this groove is illuminated. The illuminated areas of the groove surfaces are indicated by heavy lines. Figure 9 illustrates the use of the parameter p. This integer defines the sections of the lower planes, e.g. B'C', C'D', etc. Thus $p = 2$ denotes that the ray through B intersects the line C'D' at or to the right of C' and thus groove DE is illuminated. The integer p is given by

$$p = \text{truncated value of } [h(\cot i)/a + 1]$$

where $a = \frac{1}{2}d$, the width of the groove or land and h is the groove depth.

(b) Partial masking with non-absorbent grating material

The partial masking situation is particularly relevant in the shorter wavelength domain (around 0.1 nm), where the absorption of X-rays by the grating material is relatively small. The index of refraction of the reflecting material varies little from unity for these wavelengths and hence refraction is not taken into account.

Based on these considerations, it can be shown (Bennett 1971) that the diffraction efficiency of the odd orders is given by

$$E = \frac{100R}{m^2\pi^2} \left\{ 1 + \cos^2\left[\frac{m\pi h \cot i}{2a}\right] - 2\cos\left[\frac{m\pi h \cot i}{2a} + \delta'\right] \cos\left[\frac{m\pi h \cot i}{2a}\right] \right\},$$
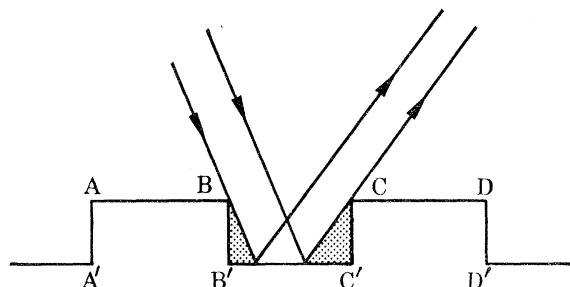
where $\delta' = 2\pi h(\sin i + \sin\theta)/\lambda$.

FIGURE 10. Full masking. The grating material is assumed to be totally absorbent.

(c) Full masking with absorbent grating material

The 'shadow' to the right-hand side of the groove in figure 10 occurs as a result of absorption in the grating material of the radiation incident on the face CC'. The emergent diffracted beam will thus contain contributions of energy diffracted from the groove bottoms only when the grooves are illuminated directly. This occurs more readily for larger incidence angles, corresponding to longer wavelengths. It is just these wavelengths which are more highly absorbed, thus giving rise to a state approaching the full masking condition.

Under these conditions it can be shown that the absolute efficiency in the odd orders is

$$E = \frac{100R}{m^2\pi^2} \left\{ 1 + \cos^2\left[\frac{m\pi h}{2a}(\cot i + \cot\theta)\right] - 2\cos\left[\frac{m\pi h}{2a}(\cot i - \cot\theta) + \delta'\right] \cos\left[\frac{m\pi h}{2a}(\cot i + \cot\theta)\right] \right\}.$$

At very shallow incidence angles and at wavelengths of about 0.1 nm, the radiation which penetrates the grating material through the barrier supporting the land areas will be partially absorbed only. For the zero order, the radiation diffracted from the groove bottom will pass

through an equal number of material barriers under the lands as the incident beam. To a first approximation, the same will apply to the subsequent spectral orders of low order number, where the dispersion is relatively small at short wavelengths. If the beams incident on the grooves each pass through j such barriers, then those diffracted beams of sufficient intensity to be of interest will also pass through j barriers. Thus the path length traversed through the grating material is given by

$$x = jd/\cos i.$$

The transmitted intensity is given by $I = I_0 \exp(-\mu_1 x)$ and hence the amplitude of the beams diffracted from the groove bottoms is therefore reduced by a factor $\xi = \exp(-\frac{1}{2}\mu_1 jd/\cos i)$. The beam will also be retarded in phase as a result of the optical path difference introduced on traversing a denser medium. The path difference

$$\delta_m = \frac{2\pi}{\lambda}(n-1)x = -\frac{2\pi}{\lambda}x\delta,$$

where n is the refractive index and δ the unit decrement.

In deriving the expressions for absolute efficiency both the amplitude and phase of the radiation diffracted from the groove bottoms must thus be modified. Introducing the factors ξ and δ_m, modifies the expression previously quoted for diffraction efficiency in odd orders for the case of partial masking, as follows:

$$E = \frac{100R}{m^2\pi^2}\left\{1 + \xi^2\cos^2\left[\frac{m\pi h \cot i}{2a}\right] - 2\xi\cos\left[\frac{m\pi h\cot i}{2a} + \delta'\right]\cos\left[\frac{m\pi h\cot i}{2a}\right]\right\}.$$

For simplicity, the theoretical discussion has been confined to gratings having equal land and groove widths. It was seen from figure 8 that the effects of shadowing were to reduce the maximum efficiency recorded in the first order (in the limit to 10 %). It is therefore advantageous to increase the groove-to-land width ratio in order to increase the contribution in the diffracted beams from the groove areas, so that the amplitudes diffracted from the top and bottom of the grooves are equal. This argument does not apply to gratings illuminated at very shallow angles and where penetration through the grating is possible, since in this case the grooves can be completely illuminated.

Ideally, therefore, a grating should be manufactured for use at a given wavelength λ and at a given incidence angle and where the groove depth h is defined by the primary maximum position defined by λ/d. Knowing these parameters, the land-to-groove width ratio should then be optimized in order to illuminate equal land and groove areas.

4. Manufacture

(a) General principles

The desired rectangular waveform is produced by ion etching a figured blank through a mask consisting of a vacuum-deposited aluminium layer, which has previously been ruled and chemically etched. The manufacturing procedure which has a success rate of over 90 % is illustrated in figure 11.

The basic principles of the manufacturing techniques are simple. However, severe experimental problems are encountered in achieving perfection at something approaching an atomic scale, but these must be overcome in order to reduce scatter to a minimum and to maintain a

516   A. FRANKS AND OTHERS

high diffraction efficiency over a wide wavelength range down to below 0.1 nm, where the incidence angles are a few minutes of arc only. Some of the techniques employed and the precautions which must be taken at each stage of the process are discussed below.

(b) *Preparation of the blank*

The grating substrate is made of Spectrosil, a synthetic amorphous silica manufactured by Thermal Syndicate Ltd and was selected after making extensive tests on a number of glasses. The criteria were ultimate surface finish, dimensional stability, chemical inertness and uniform behaviour during ion etching. Its relatively low thermal expansion coefficient is also advantageous. The glass working techniques employed are highly refined, for example, all surfaces of the blank are polished, and not left 'grey' or lightly ground as is the usual practice, because of the difficulty in cleaning a ground surface sufficiently well.

stage 1: chemical and glow discharge clean Spectrosil mirror; aluminize

2: rule

3: chemical etch

4: ion etch

5: chemically remove aluminium

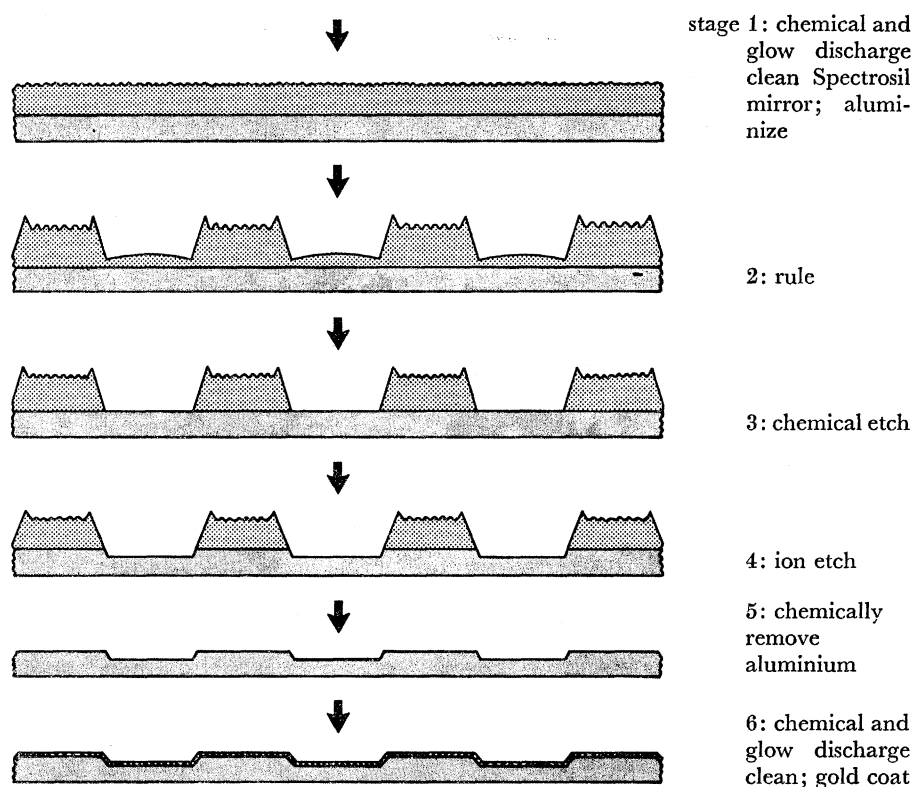6: chemical and glow discharge clean; gold coat

FIGURE 11. Stages in the manufacture of N.P.L. X-ray gratings.

The mechanisms involved in the production of the final surface topography are still not fully understood and the achievement of the requisite 'X-ray finish' is still to some extent an art and is dependent on the skill of the glass worker. Nevertheless, some important principles have been established and yield a success rate approaching 100 %. It is found that the best finish is obtained by using machine methods of polishing with a resin wheel and a ceria–water polishing medium. The path of the blank with respect to the wheel should be maximized for randomness and further randomness is introduced by employing an irregular pattern of surface relief on the polishing wheel.

(c) Cleaning the blank

Cleaning and all subsequent processing are carried out under clean room conditions.

Mechanical cleaning methods, such as scrubbing, invariably produce surface scratches and are therefore unacceptable. Cleaning is thus carried out in stirred liquids. The blank is clipped into a stainless steel holder, in which it remains during all the processes prior to ruling. The blank needs to be handled only at the ruling stage. The first cleaning liquid is 20 % 'Decon 75' (Decon Laboratories Ltd) + 80 % deionized water. This is followed by working in five changes of deionized water and ultimately freshly filtered AR grade absolute alcohol which is blown off with filtered hot air.

(d) Aluminizing

The smoothness of the grooves before and after chemical etching is closely related to the homogeneity, and thus the purity, of the aluminium layer and to its surface smoothness. The aluminium used is of 99.999 % purity.

Before deposition, the evaporator is thoroughly cleaned, the tungsten heater filament and aluminium charge are chemically pre-cleaned and then outgassed, the former at 2000 °C and the latter at 660 °C. The evaporator is glow-discharge cleaned both before and subsequent to insertion of the glass blank, the latter treatment also serves to produce a significant improvement in the adhesion of the film to the substrate.

The aluminium is evaporated slowly, typically 50 nm/min, to minimize 'spitting'. The vapour beam is collimated so that it impinges on the specimen at less than 10° off normal incidence, since surface smoothness deteriorates fairly rapidly at larger angles. Evaporation is carried out at a pressure no greater than 10^{-4} Pa, to minimize aluminium oxide formation.

(e) Ruling

The ruling engine used has been described by Stanley, Franks & Lindsey (1968).

It is desirable to minimize the total amount of aluminium to be removed during chemical etching and the grooves are thus ruled as close to the desired width as possible. The diamond tool produces grooves by metal displacement and not by a cutting mechanism. The stresses imparted to the aluminium film extend into the substrate and will cause the latter to deform plastically if a threshold pressure is exceeded. The tool to substrate separation should thus not be less than about 100 nm.

(f) Chemical etching

The etchant is 4 % Decon 75 + 96 % deionized water. Hydrogen bubbles produced have to be removed since they would mask the aluminium and cause roughening of the groove edges. Etching is thus carried out in a laminar flow bath in which velocity gradients in the region of the specimen are negligible: etching rate increasing with flow velocity. Normal flow rate is 10 mm/s. The etching assembly is shown in figure 12, plate 17. All components are made of Perspex, stainless steel or silicone rubber to reduce contamination. The etching tank is gravity fed via a flow straightening nozzle, the feed tank being replenished via a peristaltic pump. A typical total etching time is 5 min. On completion of etching, the standard washing and drying procedure is carried out, and the grating is then transferred as quickly as possible to the ion etching apparatus.

(g) Ion etching

Ion etching is carried out in a d.c. triode CVC Plasmavac equipment. To ensure uniform plasma density, the grating is mounted on a super-pure aluminium electrode having all its edges radiused and which masks the grating edges from the electric field. Argon ion bombardment is carried out at an accelerating voltage of 600 V and at a pressure of 5×10^{-2} Pa. The etching rate is about 0.05 nm/s, so that the normal etching time rarely exceeds 10 min.

(h) Removal of aluminium strips

This is accomplished by chemical dissolution in a dilute Decon solution and is followed by the standard cleaning routine.

(i) Gold coating

The technique is similar to that employed for the aluminium coating. The deposition rate is slower and is typically 0.5 nm/min.

5. Structural studies and assessment

The only reliable method of assessing the performance of a grating is by examining its X-ray spectroscopic performance under varying conditions of wavelength, grazing angle and aperture, ideally with apparatus specially designed for this purpose. However, in order to correlate X-ray performance with grating structure and profile and to monitor all stages of the manufacturing process, it is also necessary to develop other less direct methods of assessment. The techniques which are employed in addition to X-ray spectrometry are optical and electron optical microscopy, electro-mechanical profile measurement, X-ray reflectometry and to a lesser extent both ellipsometry and optical emission spectrography. This section is divided into two parts: the first deals with the subsidiary techniques and the second part with the spectroscopic instrumentation.

(a) Subsidiary assessment

The efficacy of the cleaning procedure is checked by ellipsometry, and surfaces are considered to be clean if the contamination layer is less than 0.1 nm thick. The purity of the evaporated films is determined by optical emission spectrography. The main impurities which have been detected are Cu, Si and Ca (each less than 0.05 %) and a trace of Mg (less than 0.03 %) and this impurity content is found to be acceptable.

Optical microscopy is used in all the grating manufacturing stages. Experience has shown that if any structure is visible in the microscope, other than the occasional pinhole, scratch or sleek, the grating will be inferior.

If an unruled blank passes the optical inspection test its surface finish is then examined by X-ray reflectometry, described by Lindsey (1973).

Gratings made from imperfect mirrors will display structural defects in the spectral lines and, conversely, if a mirror produces a structureless image then the grating made from the mirror will also give rise to structureless spectra. Figure 13, plate 17, is the photograph of the zero and first order spectra from a 5 m radius grating illuminated with Cu K radiation (0.154 nm), with the film displaced to intercept some of the secondary foci. Figure 14, plate 17, illustrates the corresponding spectra obtained from a good 5 m radius grating. In stage 1 of the manufacturing process, the routine method of testing the quality of the aluminized surface is by optical
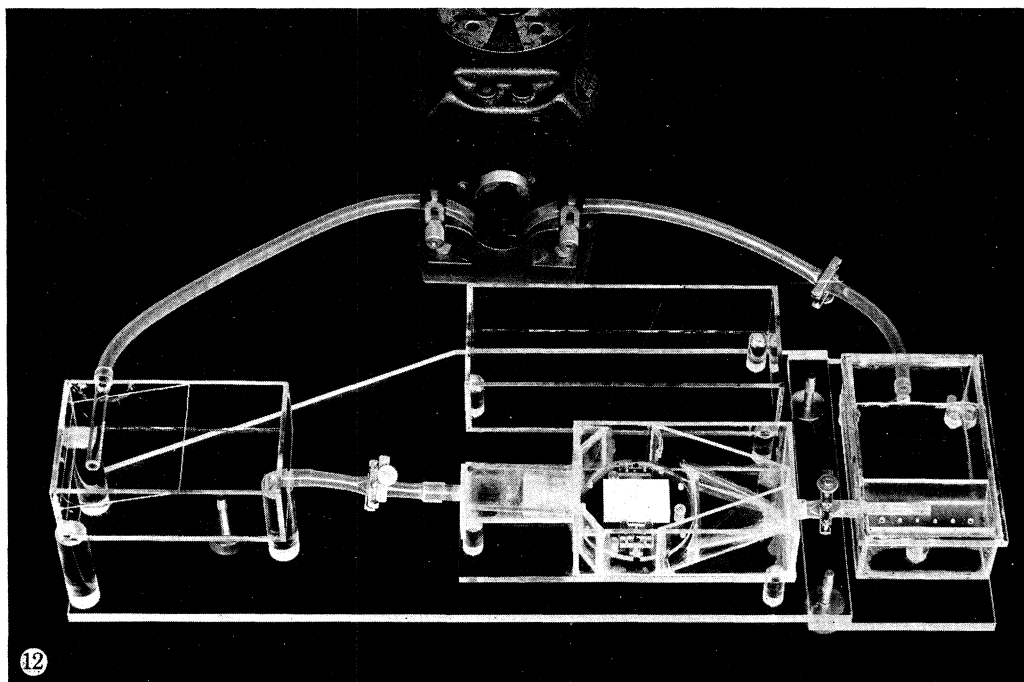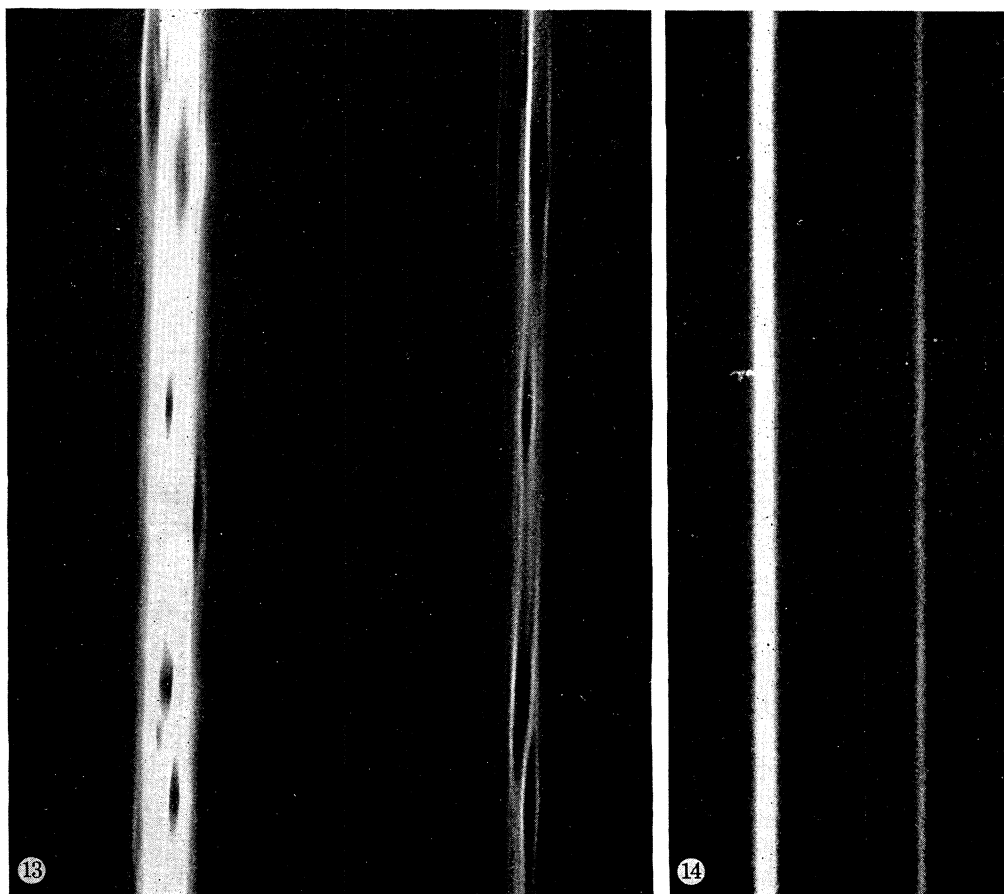
FIGURE 12. The perspex chemical etching assembly showing a grating in position in the etching bath (centre).

FIGURE 13. Structure at secondary foci in the zero and first order spectra obtained with an imperfect 5 m concave grating. (λ = 0.154 nm.)

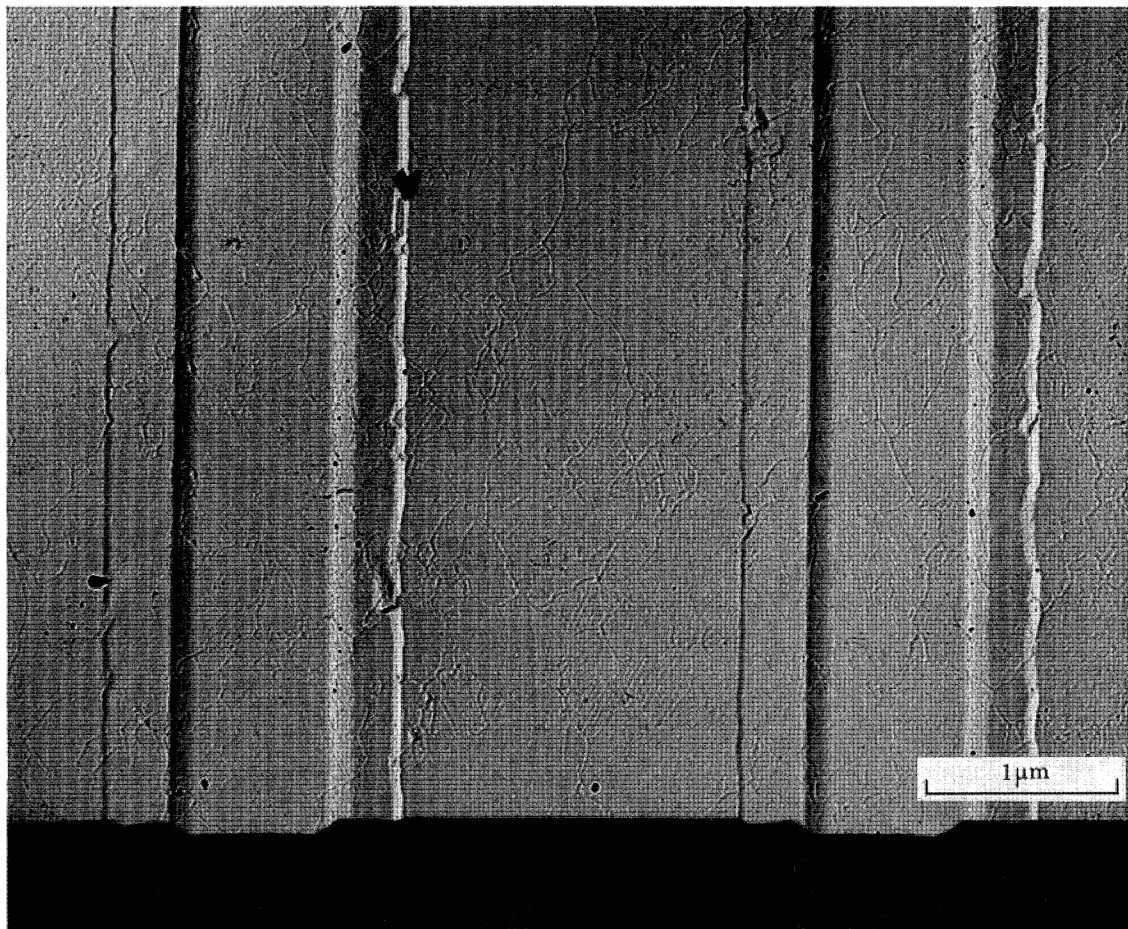FIGURE 14. Zero and first order spectra from a structure-free 5 m concave grating. (λ = 0.154 nm.)

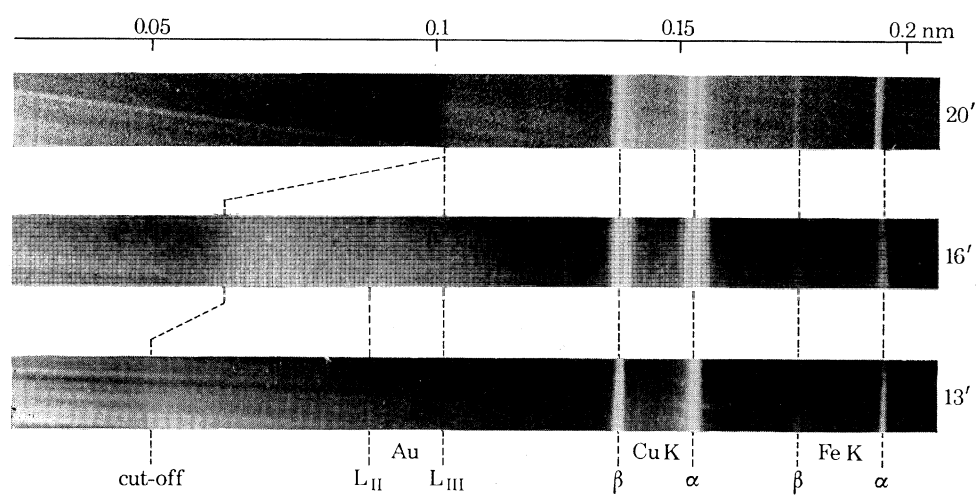FIGURE 15. Montage showing electron micrograph of a 300 lines/mm grating surface and profile.

FIGURE 41. Dependence of first order short wavelength cut-off on incidence angle.

examination under Nomarski polarization interference contrast illumination. This technique is sufficiently sensitive to give qualitative information about structural surface imperfections of amplitudes down to 3 nm. The lateral resolution is limited to sub-micrometre dimensions, so that the optical examination is occasionally supplemented by electron microscopic studies of the aluminized surface. The purpose of these studies is to maintain control over the surface smoothness of the aluminium layer, which, as explained in §4(d), is a factor which determines the groove quality of the final grating.

In the subsequent manufacturing stages up to and including the removal of aluminium after ion etching, the main assessment and inspection techniques employed are the Vickers–Dyson shearing-image eyepiece for groove width measurement and Nomarski illumination for surface structural examination. Considerable effort has been expended on devising suitable techniques for measuring the profile and particularly the groove depth of the ion-etched grating. Since groove depths are typically in the range 5–50 nm, two-beam interference microscopy does not give sufficiently accurate results. Multiple beam interferometry is not practicable because the grooves must be examined at high lateral magnification. It is not easy to make either scanning or conventional transmission electron microscopy quantitative, but the latter technique is extremely useful to give an overall picture of the grating, especially when it is used together with a more quantitative technique.

Three electron microscope replica techniques have been employed with a certain measure of success, the first two methods have been described by Bennett (1969), the third by Butler (1973).

Figure 15, plate 18, is a montage of a general view of a grating surface, obtained by conventional two stage replication and carbon–platinum shadowing, and a silhouette obtained by the bending technique. The groove shape is not obvious from the general view and there is little indication of the slopes of the shoulders on either side of the groove, although these are clearly visible in profile in the lower part of the figure. The fine structure visible over the grating surface is replica and not grating structure. This replica structure limits the usefulness of electron microscopy for studying smooth surfaces.

Butler's (1973) technique consists of measuring the relative heights of electron absorbent particles 'decorating' an electron transparent replica of the grating by examination of the parallax between two stereoscopic photographs of the decorated replica. The vertical resolution with this technique is 0.5 nm while the lateral resolution of the electron microscope can be exceeded because of the additional information which is available in stereoscopic viewing.

There is considerable uncertainty about the accuracy attainable with these techniques described because the replicas tend to distort.

The most direct and reliable method of determining groove depth and, at least, the major features of the profile is by use of a modified Rank Precision Instrument Company 'Talystep' measuring machine (Verrill 1973). An extra fine diamond stylus is used having a width of 100 nm and an included angle at the apex of 90°. The main modification to the instrument is that the lateral magnification has been increased by a factor of 20, so that the lateral resolution is about 100 nm and the vertical resolution approaches 0.5 nm. The profile of the steep shoulder of the grooves is not faithfully reproduced because of the large included angle of the tool, but it can be deduced from both knowledge of the tool shape and the form of the groove obtained electron microscopically. A 'Talystep' profile of a grating is shown in figure 16.

53

(*b*) *Spectroscopic instrumentation*

The X-ray spectroscopic assessment of the gratings was carried out with four instruments: two spectrometers at N.P.L., a grating analyser at Imperial College and a spectrograph at the Atomic Weapons Research Establishment. The main purpose of this assessment was to determine absolute diffraction efficiencies of gratings under different conditions.
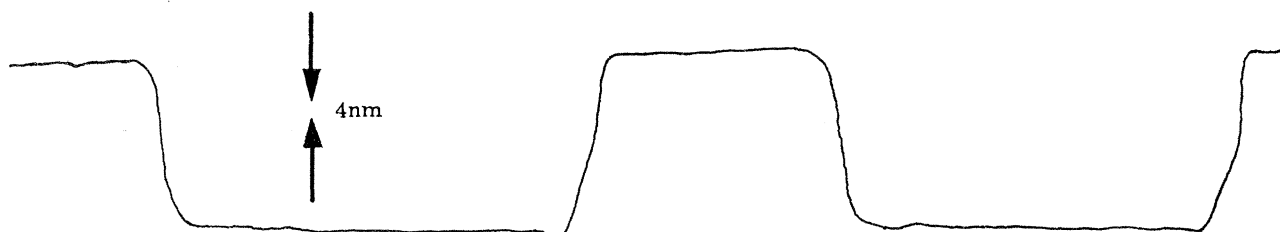

4nm

FIGURE 16. Talystep profile of a 300 lines/mm X-ray grating.

(i) *The N.P.L. hard X-ray spectrometer*

This spectrometer has been used in the wavelength range of 0.056 nm (Ag K)–0.54 nm (Mo L). The spectrometer is normally run in air except when it is used with wavelengths greater than 0.3 nm, for which air absorption is appreciable. For these larger wavelengths the instrument is maintained in a helium atmosphere.

The X-ray source is a Hilger 'Microfocus' X-ray tube having interchangeable anodes. The effective source size is 60 μm × 7 μm and maximum rating is 500 μA at 50 kV. The spectrometer is illustrated in figure 17.

Under typical working conditions, the double slit collimator restricts the divergence of the incident beam to 5″ and the width of grating illuminated will be between 1 and 2 mm. This allows the grating to be scanned across the beam to enable it to be tested for uniformity. The grating can be retracted to facilitate measurement of the incident intensity with the proportional counter. The diffraction efficiency is obtained by comparison of the total intensity in the diffracted beam of any order and of the incident intensity.

dial gauge

dial gauge

X-ray source   collimator

goniometer – mounted
grating

film
cassette

proportional
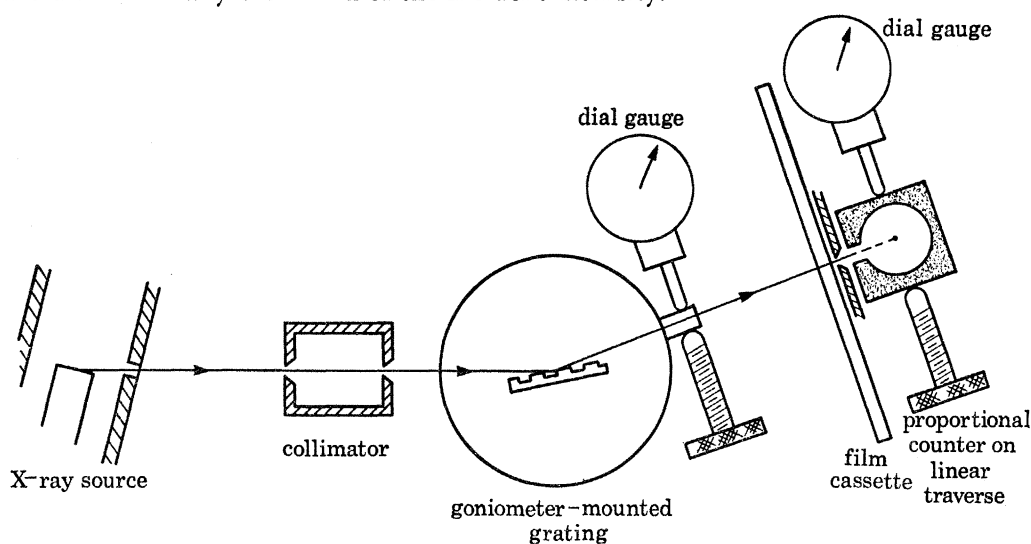counter on
linear
traverse

FIGURE 17. The N.P.L. hard X-ray spectrometer.

The incident radiation is not monochromatic but consists of a characteristic spectral line superimposed on a white radiation background. The ratio of the diffracted and direct beam intensities would thus give a low value of diffraction efficiency. This error is reduced by feeding the output of the proportional counter to a pulse height analyser, prior to measurement of intensities with a scaler, thus effectively monochromatizing the incident radiation.

The photographic attachment to the spectrometer is used extensively to assess the quality of the gratings. The spectral photographs (figures 13 and 14, plate 17) were obtained with this instrument.

(ii) *The N.P.L. soft X-ray spectrometer*

This is a vacuum spectrometer similar to the hard X-ray spectrometer, but it is housed in a nickel plated mild steel vacuum tank, with the spectrometer mechanism suspended from the tank lid. It has been used principally at wavelengths of 0.83 nm (Al K) and 4.45 nm (C K). X-radiation is generated by a separately pumped X-ray tube, with interchangeable anodes, which may be isolated from the spectrometer to allow independent evacuation of the tank.
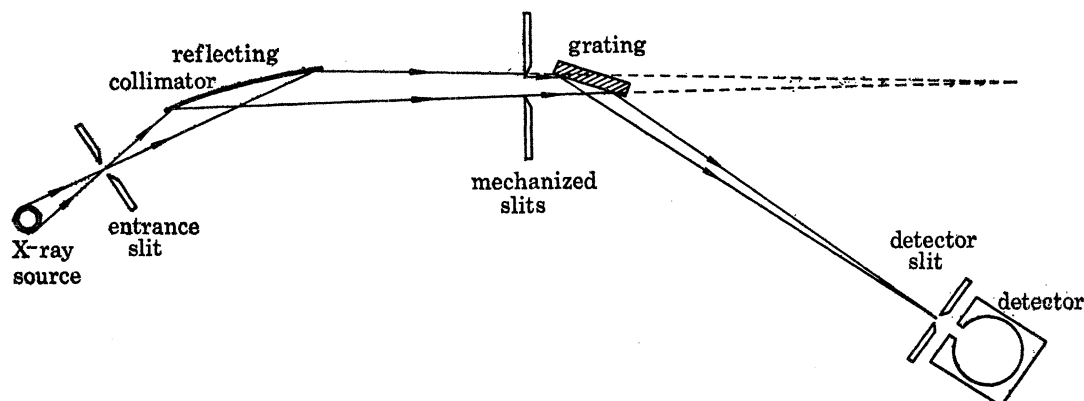
FIGURE 18. Diagram of I.C. grating analyser.

(iii) *The I.C. grating analyser*

This is a vacuum instrument (Speer 1970) built on a large scale to enhance its versatility. It has been used principally at 0.83, 2.3 and 4.45 nm (Speer & Turner 1973). The optical arrangement is shown in figure 18. When used for testing plane gratings a novel collimation system is employed, enabling the grating to be illuminated by an approximately parallel or slightly convergent beam. The collimator is a reflecting gold coated float glass plate, shaped so that when bent in a cantilever mode it forms part of a right elliptical cylinder. With the entrance slit placed at one focus of the ellipse, the emergent beam converges to the other, at a distance of a metre or so. By careful choice of the angle of incidence of the radiation from the source onto the reflector, some suppression of short wavelength impurities in the radiation may be achieved.

An essential feature of the apparatus is the facility to retract the grating out of the beam, by control from outside the vacuum vessel. This makes it possible for absolute diffraction efficiency measurements to be made by measuring the intensity of the beam incident on the grating.

The detector is a Bendix magnetic electron multiplier, which is driven in orthogonal X–Y coordinates by leadscrews to scan the image area. An experimental scan is normally made by stepping the detector, under automatic control, in the Y ordinate, first across the direct beam,

and then across the negative orders, zero order, and positive orders of interest. The grating is replaced in the beam without interrupting the scan as soon as the direct beam has been traversed. This gives a useful record of the prevailing level of instrumental background noise (usually a count of below 10/s) in the shadow area behind the projected plane of the grating surface.

(iv) *The A.W.R.E. spectrograph*

This instrument was required by the U.K.A.E.A. Culham Laboratory to recover spectra between 0.05 and 5 nm from short-lived, high temperature plasmas. A focusing grazing incidence spectrograph (Speer, Peacock, Waller & Osborne 1970) was constructed as a result of collaboration between N.P.L., Imperial College, Culham Laboratory and A.W.R.E. It was designed around an N.P.L. concave grating of 5 m radius, a ruling frequency of 300 lines/mm and a working area of 10 mm × 10 mm.

With a 10 mm ruled width of grating, the resolution is limited by the main slit width. In practice, slit widths of a few micrometres can be achieved with uniform transmission.

The photographic plates normally used are Ilford Q2 or Kodak–Pathe SC-7 which is 9 times more sensitive. The Eastman–Kodak 101-05 emulsion is even more sensitive but it is unreliable for photometric work since its characteristics vary from batch to batch and its sensitivity is very dependent on development conditions.

n	λ/nm
3	4.45
2	4.45
1	4.45
2	0.83
1	0.83
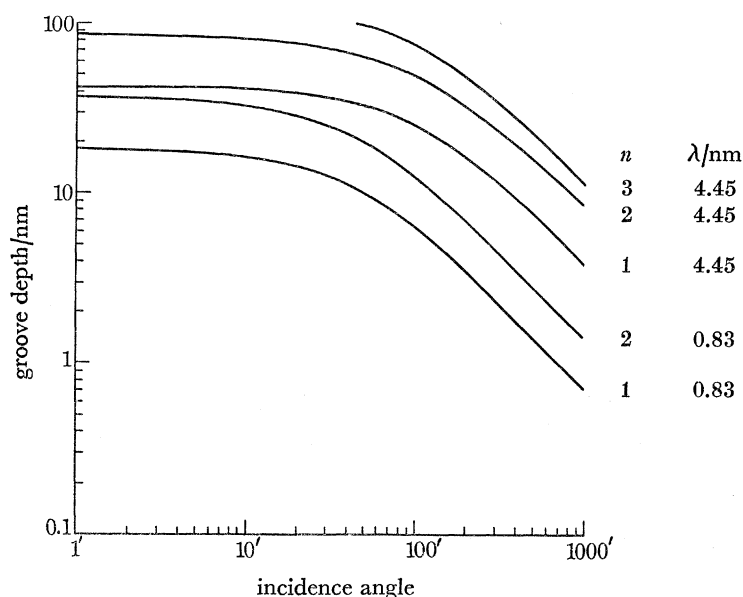
FIGURE 19. Relation between groove depth and incidence angle for the primary maximum, first minimum and second maximum of efficiency in the first order ($m = +1$), for a 300 lines/mm grating.

6. RESULTS AND DISCUSSION

(a) *Performance at* 0.83 nm *and* 4.45 nm

In the results to be shown, the absolute efficiency is plotted as a function of grazing incidence angle i for two wavelengths, first at $\lambda = 4.45$ nm (C K radiation) and secondly at $\lambda = 0.83$ nm (Al K radiation). These are discussed in turn in relation to the theory developed earlier in §3, with particular reference to the groove depths of the respective gratings. A number of maxima

and minima which occur in the first spectral order ($m = +1$) diffraction efficiency curves for the range of groove depths used are identified by means of figure 19. This figure shows a graph of the groove depth of a phase grating plotted as a function of grazing incidence angle for the primary maximum, first minimum, and second maximum of efficiency (i.e. for $n = 1, 2,$ and $3,$ respectively (see equation (2))) in the first order at $\lambda = 4.45$ nm and $\lambda = 0.83$ nm for rulings of 300 lines/mm.

At relatively large angles of grazing incidence (typically angles in excess of $3°$), the shadowing effects in the grooves are small, and useful contributions to the diffracted energy will be experienced from a large proportion of each groove. Large grazing incidence angles will give a highly reflected beam only if the wavelength of the coherently scattered radiation is greater than about 3 nm. It is, therefore, advantageous to use the C K radiation at 4.45 nm in the first instance to test the theory developed, where the grooves are directly illuminated by the incident radiation.

Figures illustrating performance at $\lambda = 4.45$ nm were obtained with the aid of the N.P.L. soft X-ray spectrometer. The small diagrams of the grating profiles inset in the figures illustrate the angles i_1 and i_2 at which the grooves for that particular grating are (a) completely shadowed by the preceding land areas (i_1) so that there is no contribution from the grooves at this angle, and (b) only half shadowed so that the reflected beams start to emerge from the grooves (i_2). The two angular positions are indicated on the i-axis by arrows at the appropriate positions.

Figure 20a illustrates the diffraction performance as a function of grazing incidence angle of a grating with a groove depth of approximately 18 nm, before gold coating (N.P.L. grating no. 83), in the zero ($m = 0$) and first ($m = +1$) spectral orders. A well defined maximum is seen in the first order slightly displaced in the direction of decreasing i with respect to a minimum in the zero order.

The broad first order experimental peak shown in this figure corresponds to the primary maximum of efficiency. It is slightly displaced in the direction of decreasing i with respect to its predicted position from figure 19 at approximately $i = 3° 30'$ for a groove depth $h = 15$ nm as a result of the reflectivity factor which decreases with increasing i.

The absorption of C K radiation ($\lambda = 4.45$ nm) in gold is such that the intensity of a transmitted beam is reduced by $1/e$ in a distance of about 2 nm. In this instance, no significant contributions to the diffracted energy will therefore be experienced from the areas of the grooves that are masked by the land areas on either side of each groove. The full masking model should, therefore, be a good approximation in this case.

Predictions of the performance at different groove depths based on the full masking model in both the zero and first orders are shown in figures 20b, c, respectively. By a comparison of the position of the zero order minimum with those of the predicted curves, a groove depth $h \approx 15$ nm is seen to give good agreement, while the first order maximum also corresponds well to $h \approx 15$ nm in figure 20c. The maximum in the zero order predicted at $i \approx 1° 30'$ in figure 20b results from the total masking of the groove as i decreases. No experimental maximum is observed in this region since the groove was considerably wider than the land (land/groove ratio of about 0.6), so that the groove did not become completely masked until i was less than $1°$ (as indicated by i_2 in figure 20a). Also, the intensity of the reflected beam at shallow grazing angles increased as a result of the fixed divergent incident beam illuminating the unruled areas of the grating blank. This also caused an apparent drop in the recorded diffraction efficiency in the first order. For this latter reason the experimental performance figures obtained by using the N.P.L. soft X-ray spectrometer were considered unreliable at grazing angles less than $1°$.

The theoretically predicted curves for the first order performance are seen to be smooth, as would be expected from the computation of the function defining the efficiency. However, undulations were recorded at the peak of the first order experimental curve (figure 20a) which are outside the errors indicated, the latter being determined by the incident beam fluctuations plus the statistical variation. The undulations were also reproduced during completely independent recordings. A possible explanation of their occurrence may lie in the effects of interference between those fractions of radiation reflected from the vacuum–gold interface and the gold-substrate interface of a gold coated grating, normally known as Kiessig interference patterns (Kiessig 1931).

A deeper grooved grating (N.P.L. grating no. 87), showing marked oscillations in the performance curves of the zeroth and first orders (figure 21a), serves to illustrate further the correlation between theory and experiment in the present context. The groove depth, before gold
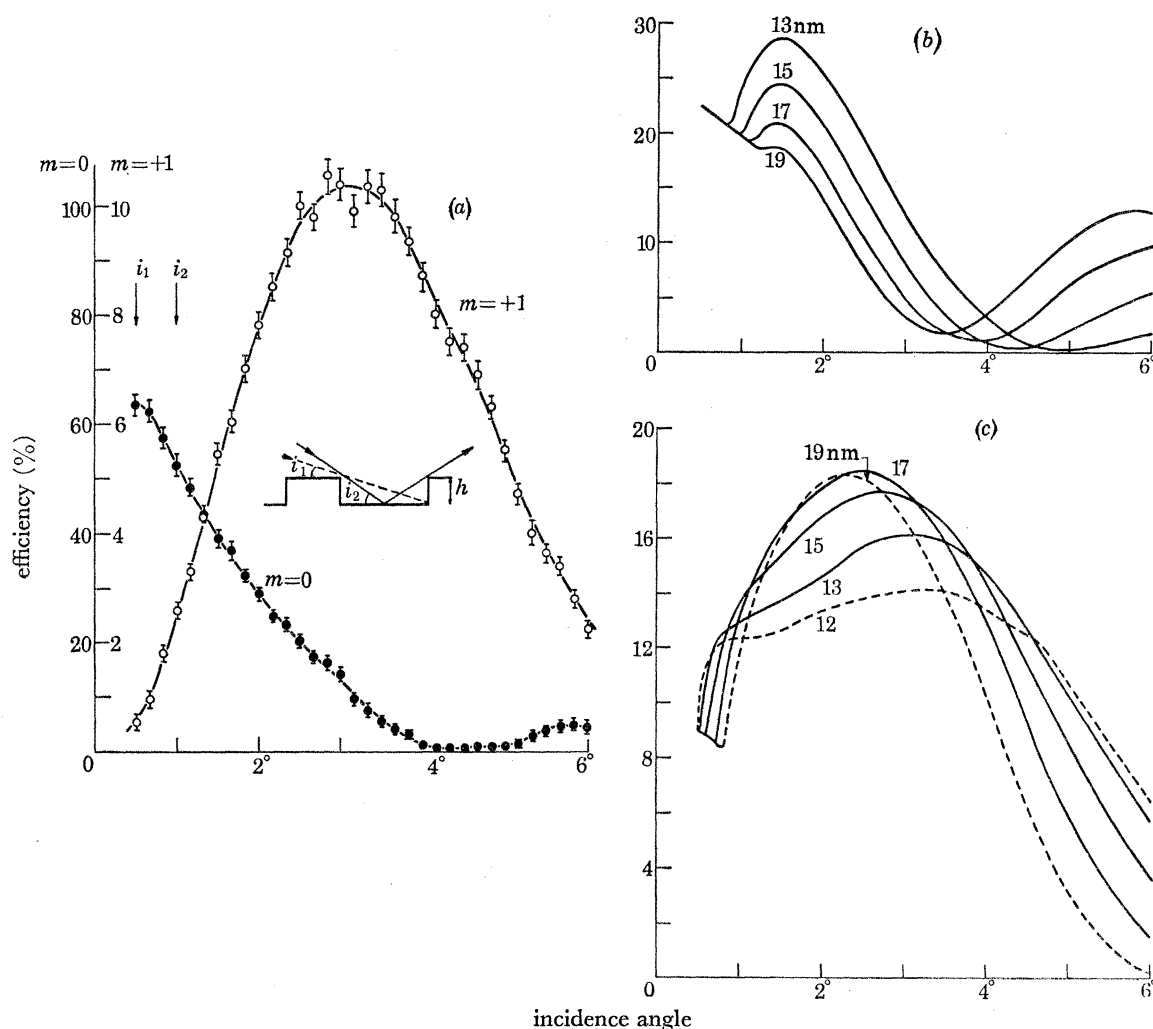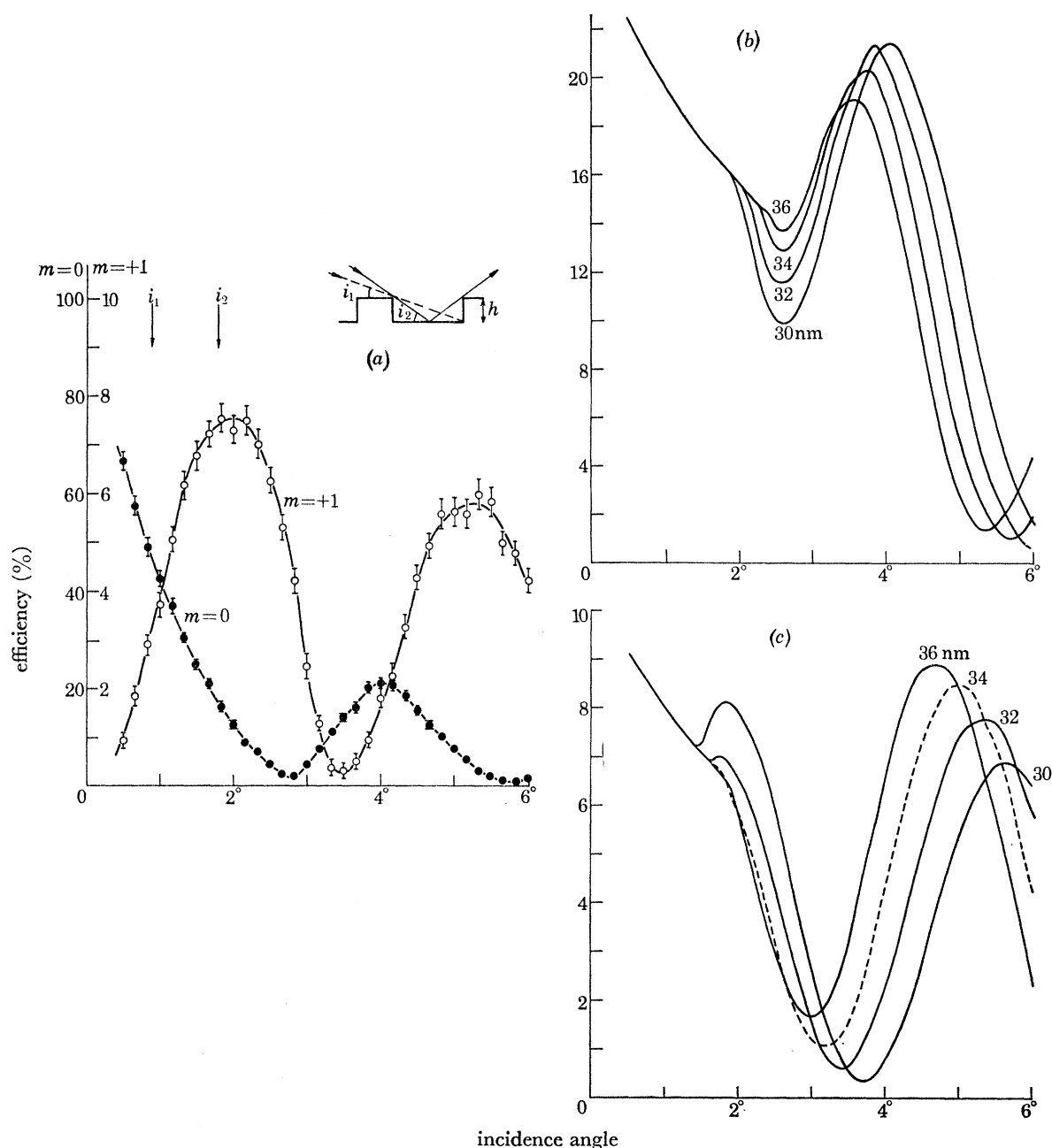

FIGURE 20. (a) Measured variation of zero and first order ($m = +1$) diffraction efficiencies with incidence angle at 4.45 nm. $h = 18 \pm 2$ nm, $i_1 = 0.5° \pm 0.05°$ and $i_2 = 1° \pm 0.1°$. (b) Calculated variation of zero order efficiency with incidence angle at 4.45 nm, for various groove depths h. Full masking model. (c) Calculated variation of first order ($m = +1$) diffraction efficiency with incidence angle at 4.45 nm, for various groove depths h. Full masking model.

coating, was in the range 30–35 nm. The displacement of the maxima and minima in the first order in the direction of decreasing i with respect to the minima and maxima respectively, in the zero order is well defined, the significance of which has already been cited in the above discussion. The theoretically predicted performance curves for different groove depths are shown in figures 21b, c for the zero and first orders respectively, according to the full masking

FIGURE 21. (a) Measured variation of zero and first order ($m = +1$) diffraction efficiencies with incidence angle at 4.45 nm. $h = 35 \pm 4$ nm. $i_1 = 0.9° \pm 0.1°$ and $i_2 = 1.8° \pm 0.2°$. (b) Calculated variation of zero order efficiencies with incidence angle at 4.45 nm, for various groove depths h. Full masking model. (c) Calculated variation of first order ($m = +1$) diffraction efficiencies with incidence angle at 4.45 nm, for various groove depths h. Full masking model.

model. Comparison of the experimental and theoretical curves is made by aligning the corresponding maxima and minima. It is found that a groove depth of about 31 nm gives good agreement in both the zero and first order curves in this instance. Once again the drop in the recorded efficiency in the first order, at incidence angles less than $1°$, is attributed to the illumination of the unruled portion of the grating by the divergent incident beam, such that only a fraction of the incident radiation illuminates the rulings and thus a pessimistic value of the performance is obtained.

The significance of the two maxima and single minimum in the first order performance curve is determined in conjunction with figure 19. For a groove depth $h \approx 31$ nm the primary maximum ($n = 1$) will occur at $i = 1°$; the first minimum ($n = 2$) at $i = 3° 30'$; and the second maximum ($n = 3$) at $i = 5° 50'$. From figure 21a it is seen that the two latter values fit very well, allowing for the slight displacement in the direction of decreasing i as a result of the reflectivity factor, but the first maximum is seen to occur at $i \approx 2°$. This is in fact the primary maximum of efficiency (where $n = 1$), but where the increase in efficiency in the direction of decreasing i is cut off prematurely as a result of the masking of the grooves, as indicated by i_2 at $i = 1° 48'$ in figure 21a.

In the foregoing results the predictions based on the full masking model developed earlier are found to give excellent qualitative agreement with the experimental results at $\lambda = 4.45$ nm. At shorter wavelengths the absorption of the radiation by the grating material decreases such that, at $\lambda = 0.83$ nm (Al K radiation), the intensity of the transmitted beam is reduced by $1/e$ in a distance of about 300 nm. Thus, for groove depths of less than about 200 nm, it is clear that a considerable contribution to the total diffracted energy in a given direction could be experienced from the masked groove areas by the penetration of the radiation coherently scattered from the grooves through the corners of the land areas. In the case of Al K radiation at 0.83 nm, the model which specifies the groove areas from which 'useful' contributions to the total diffracted energy are experienced, lies between the two limiting situations of the full and partial masking models.

To illustrate this effect of penetration of radiation through the grating material, the performance curves (efficiency against incidence angle) for a relatively deep groove grating, obtained by using the Imperial College grating analyser are shown in figures 22a and 23a. Here the groove depth of the gold-coated grating (N.P.L. grating no. 87) was in the range 30–35 nm, while the grazing angles used were less than $i = 3°$. The masking effects in the grooves were therefore large, and the grooves were completely shadowed by their contiguous land areas at $i < 1° 48'$, as depicted by angle i_2 in figure 22a.

The zero order experimental curve is shown in figure 22a. Here useful contributions to the diffracted energy are experienced from the grooves at about $i = 1° 10'$. From the small diagram in this figure illustrating the angles, i_1 and i_2, for a land-to-groove width ratio and groove depth here considered, it is seen that contributions from the grooves at $i < i_2$ can be experienced only if the coherently scattered radiation from the grooves penetrates the grating material supporting the land areas to the right hand side of each groove (while the grating is illuminated from the left). The contributions experienced at $i = 1° 10'$ are, therefore, a result of penetration of the radiation through the material barriers.

This is an important result in that it shows that, provided the radiation is not too highly absorbed by the grating material, significant contributions from deep grooves can be experienced, thus enhancing the overall diffraction efficiency. This is particularly important at wave-

lengths $\lambda \approx 0.1$ nm where shallow angles of grazing incidence are necessary (typically $i \approx 20'$) and where the masking effects to the left of the groove obscure the whole groove (i.e. $i < i_1$). In this instance, penetration into the next or subsequent grooves must then be considered, as already discussed in the development of the theoretical model.
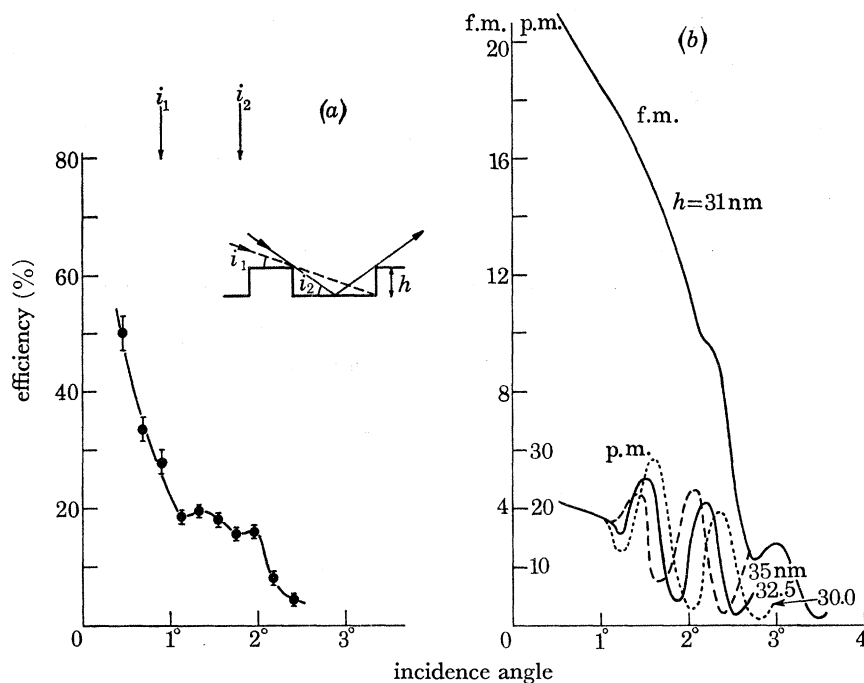

FIGURE 22. (a) Measured variation of zero order efficiency with incidence angle at 0.83 nm. $h = 35 \pm 4$ nm, $i_1 = 0.9° \pm 0.1°$ and $i_2 = 1.8° \pm 0.2°$. (b) Calculated variation of zero order efficiences with incidence angle at 0.83 nm, for various groove depths h. Full masking (f.m.) and partial masking (p.m.) models.

A comparison of the experimental results with the predictions based on the partial masking model (p.m.) will therefore be considered here, where these predictions for the zero order are shown in figure 22 b along with a single curve (plotted on a different scale for clarity) based on the full masking model (f.m.). The full masking curve, showing a kink at $i \approx 2° \ 10'$ as a result of contributions to the diffracted energy from the grooves coming into play, bears little resemblance to the experimental curve. On the other hand, the undulations of the experimental curve form very much the pattern one could expect if a 'smoothed' or 'averaged' version of the partial masking curves shown was used for comparison. At this relatively short wavelength and with a deep groove, the efficiency is a fairly fast varying function with respect to grazing angle i and groove depth h, as seen in figure 22 b. It is therefore rather difficult to give an accurate estimate of groove depth, since the surface undulations of the land and groove areas, and therefore the groove depth, is probably of the order of $\pm 1 - 2$ nm. The effect of this would be to merge the theoretical curves over a range of groove depths into a single 'averaged' curve. However, $h \sim 32$ nm would seem a reasonable average estimate.

The first orders ($m = +1$ and $m = -1$) shown in figure 23 a, illustrate similar oscillatory behaviour. The fall in performance for increasing i for $i < 1°$, in the first positive order ($m = +1$) is explained by the fact that the grooves are not illuminated, as indicated by the position of i_1, at $i = 54'$. Again an 'averaged' version of the respective predicted curves shown in figure 23 b for both $m = +1$ and $m = -1$, depict the pattern of the performance in the

respective positive orders. A groove depth in the range 30–34 nm would therefore seem a reasonable estimate from these curves, an average of which gives $h \approx 32$ nm.

One further illustration of the excellent qualitative agreement between the experimental and predicted curves is shown in figures 24 and 25. Here the performance curves in the first orders, $m = +1$ and $m = -1$, are shown for three shallow groove gratings with groove depths before gold coating of 3 nm, 6.5 nm, and 11 nm. Figure 24a shows the experimental performance curves in the first positive order for the three gratings (nos 76, 77, and 78, increasing in groove depth with grating number) together with the predicted curves, according to the full masking model, in figure 24b. (In the case of the shallow grooves considered here, the full masking model at $\lambda = 0.83$ nm gives a good approximation to the experimental performance, since the masking effects are small, and thus useful contributions from the masked areas themselves are almost insignificant in relation to that from the rest of the groove width. The full and partial
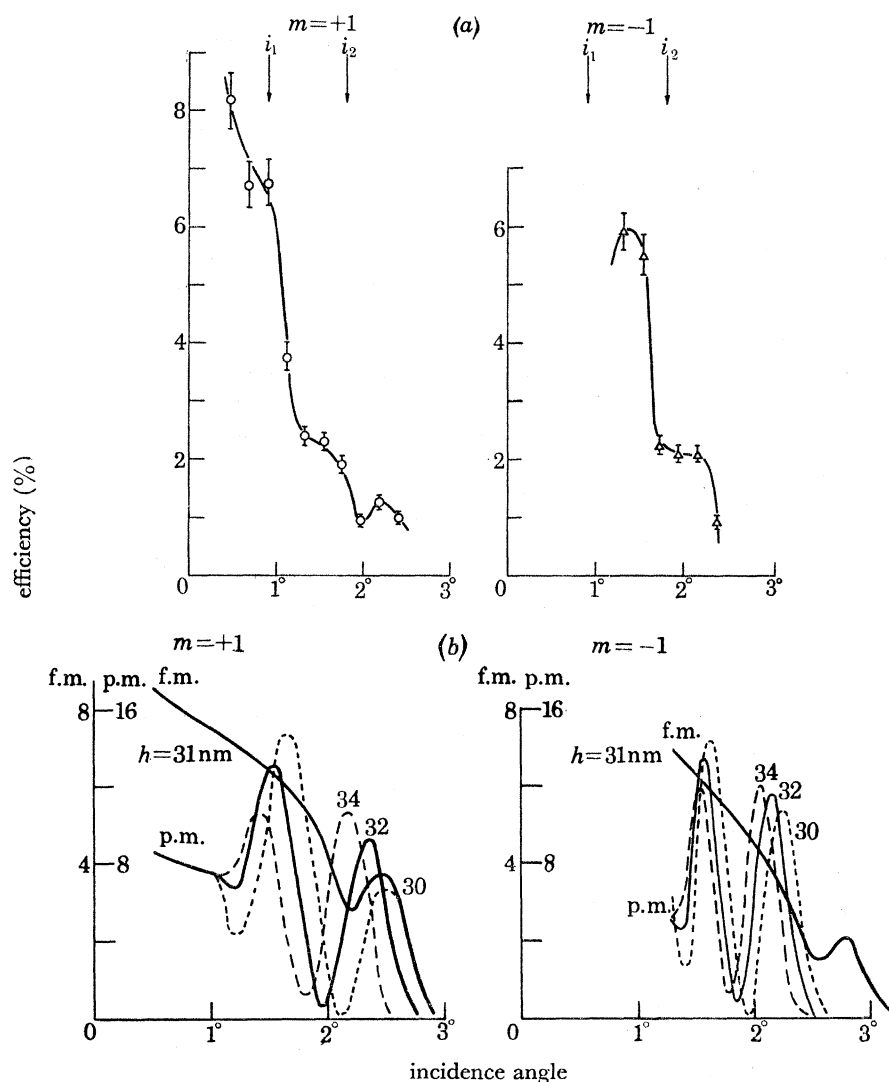
FIGURE 23. (a) Measured variation of first order ($m = +1$ and $m = -1$) diffraction efficiencies with incidence angle at 0.83 nm. (b) Calculated variation of first order ($m = +1$ and $m = -1$) diffraction efficiencies with incidence angle at 0.83 nm, for various groove depths h. Full and partial masking model.
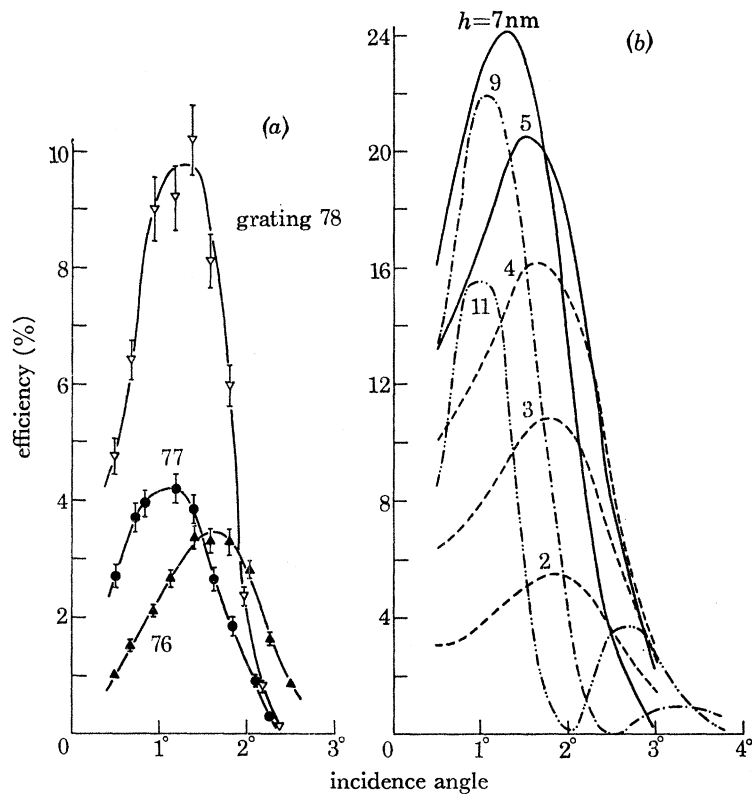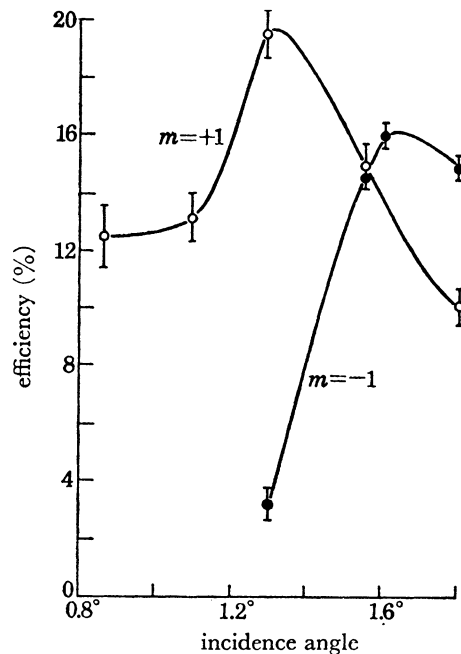
FIGURE 24. (a) Measured variation of first order ($m = +1$) diffraction efficiencies with incidence angle at 0.83 nm, for three gratings of different groove depths. (b) Calculated variation of first order ($m = +1$) diffraction efficiencies with incidence angle at 0.83 nm, for gratings of different groove depths h. Full masking model.
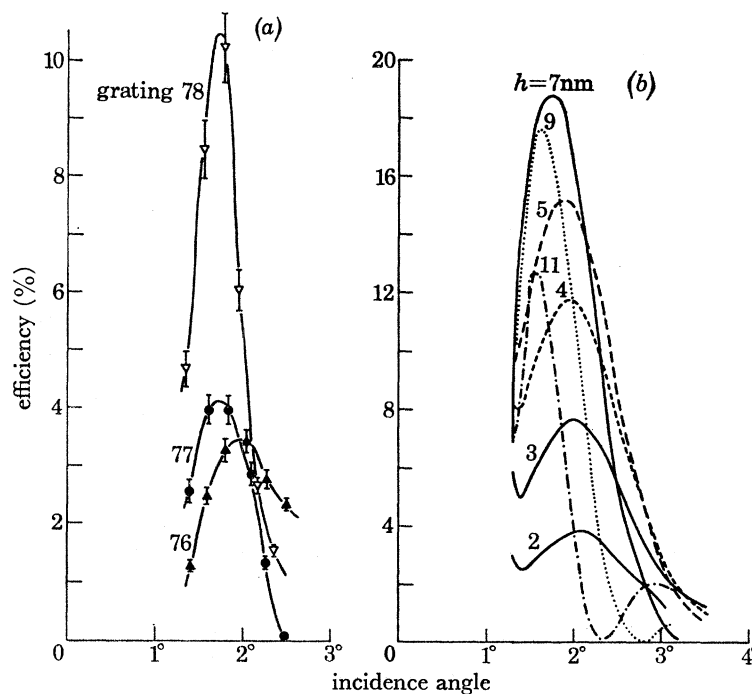
FIGURE 25. (a) Measured variation of first order ($m = -1$) diffraction efficiencies with incidence angle at 0.83 nm, for three gratings of different groove depths. (b) Calculated variation of first order ($m = -1$) diffraction efficiencies with incidence angle at 0.83 nm, for gratings of different groove depths h. Full masking model.

masking curves are, in fact, only slightly different in this instance.) The first negative order performance curves for the same gratings, together with their predicted performance, are shown in figures 25 a and b respectively. The qualitative agreement in both figures 24 and 25 is good, showing the general trends in the performance curves with a change in groove depth. Maximum absolute efficiences recorded in both the first orders ($m = \pm 1$) are in excess of 10 %.

FIGURE 26. Measured variation of first order ($m = \pm 1$) diffraction efficiencies with incidence angle at 0.83 nm, for a groove depth of 9 nm.

Figure 26 shows the experimental curve for grating no. 88 for the first orders $m = +1$ and $m = -1$. The groove depth is close to the optimum value (approximately 9 nm) and the diffraction efficiencies obtained, nearly 20 % for $m = +1$ and 16 % for $m = -1$, are virtually equal to the predicted theoretical diffraction efficiencies of figures 24 b and 25 b.

Figures 27 and 28 illustrate the performance of two gratings (with groove depths of about 15 and 32 nm respectively) in the spectral orders $m = -2, -1, +1, +2$ and $+3$. The efficiency in the respective orders is plotted on a logarithmic scale in order to show more clearly the variation in efficiency of the spectral orders. The errors on each point are as indicated in figure 25 a (i.e. $2\sigma = \pm 6$ %). The oscillatory nature of the $m = +1$ curve in figure 27 can be attributed to the properties of the phase grating, but it is seen that abrupt changes in intensity in both the orders $m = +2$ and $+3$ coincide with a fall in intensity at about $i = 1° 10'$ in order $m = +1$. At about $i = 1° 15'$ the order $m = -1$ emerges from the grating at grazing angle and, although the points are well spaced, it is clear that the intensity of the whole spectrum falls in this region. This abrupt change is noted mainly in the order $m = +2$ where a sharp discontinuity is observed. Since the characteristic oscillations of the performance curves as a result of the phase effects are smooth, the abrupt change in the whole spectrum seen here could be (partly) attributed to a Wood's anomaly (Wood 1902, 1912, 1935). The anomalies found, for
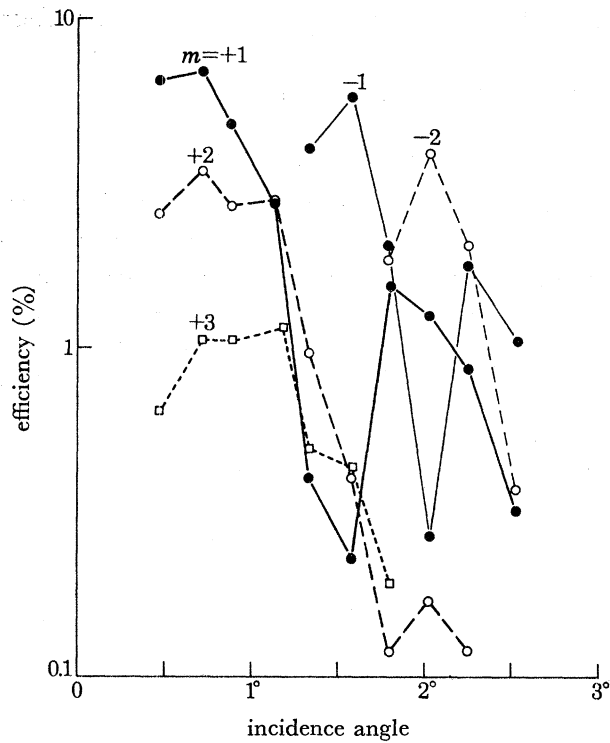
FIGURE 27. Measured variation of diffraction efficiencies with incidence angle in the spectral orders $m = -2, -1, +1, +2$ and $+3$ at 0.83 nm, for a groove depth of 15 nm.
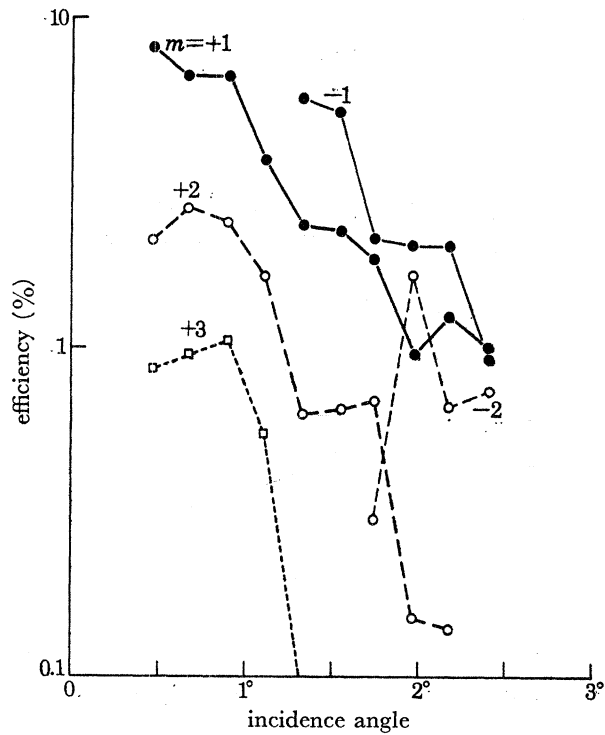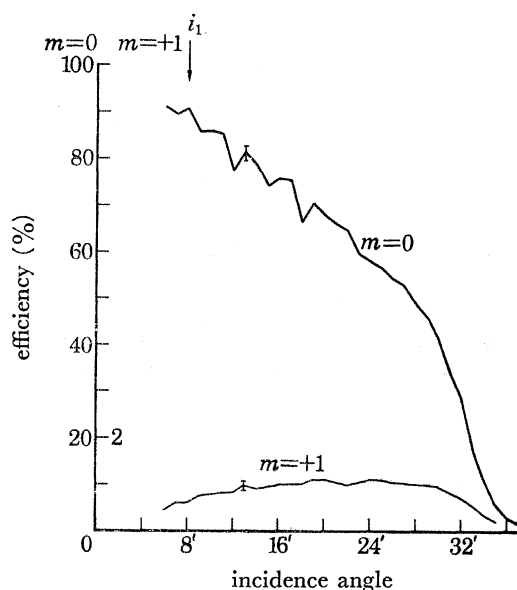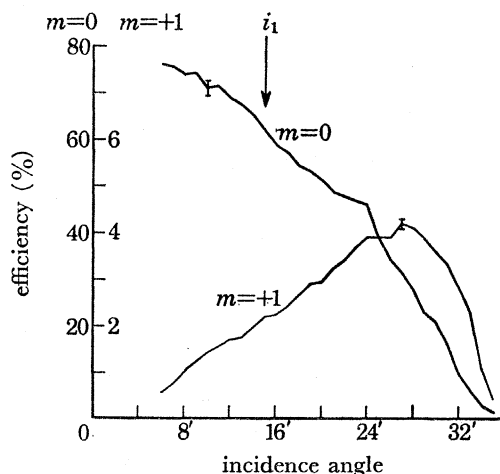

FIGURE 28. Measured variation of diffraction efficiencies with incidence angle in the spectral orders $m = -2, -1, +1, +2$ and $+3$ at 0.83 nm, for a groove depth of 32 nm.

example, by Palmer (1952, 1956) indicate that the magnitude of the effect is smaller than that experienced here, which would suggest that the phase grating characteristics are the dominant controlling factors with regard to grating performance.

(b) Performance at 0.154 nm

The results obtained with Cu K radiation at $\lambda = 0.154$ nm will be discussed in terms of the partial masking model which takes into account the penetration of the radiation through the material supporting the land areas, such that the next or subsequent grooves are illuminated. The absorption coefficient of the medium through which the radiation passes is also taken into account (where the beam passes through gold it is reduced by a factor of $1/e$ in approximately 2.5 μm), together with the phase retardation of the beam transmitted through the
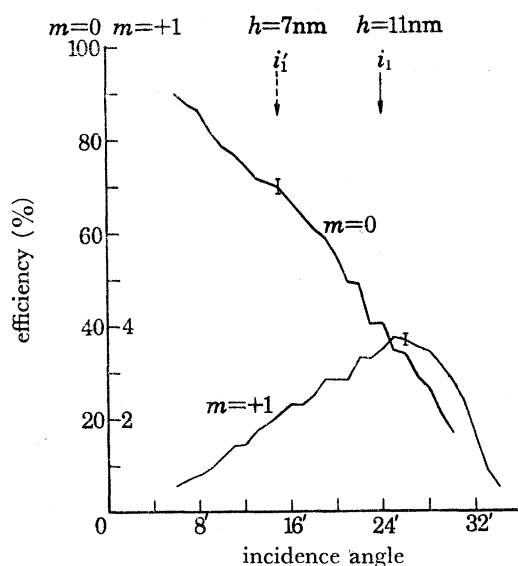

FIGURE 29. Measured variation of zero and first order ($m = +1$) diffraction efficiencies with incidence angle at 0.154 nm, for groove depth of 3 nm.

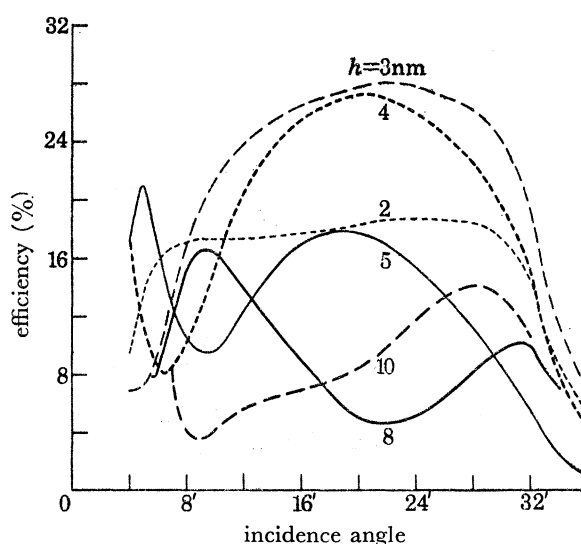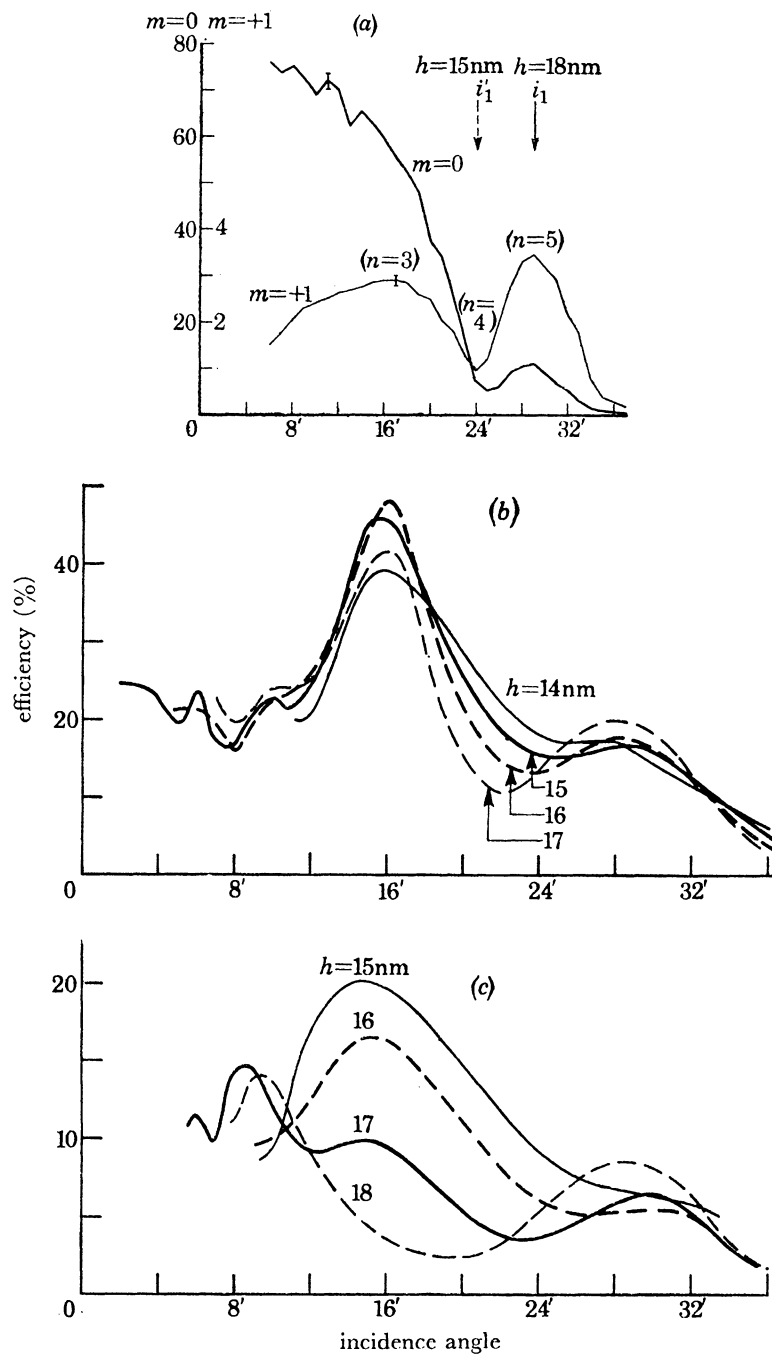FIGURE 30. Measured variation of zero and first order ($m = +1$) diffraction efficiencies with incidence angle at 0.154 nm, for a groove depth of 6.5 nm.

material which is given by $\delta_m = 2\pi(n-1)/\lambda$ (see §3(a)) where n is the refractive index of the medium. The optical path difference introduced as a result of this transmission through $2\,\mu\text{m}$ of gold at $\lambda = 0.154\,\text{nm}$ is approximately $\frac{1}{2}\lambda$.

The performance curves for the three shallower groove gratings, nos 76, 77 and 78, are shown in figures 29, 30 and 31 respectively, where both the zero and first orders are shown in each case, the estimated error at each point is ± 2–3 %. Also indicated in each figure is the angle i_1 (determined electron microscopically) at which the land area to one side of a groove just completely masks the contiguous groove from the incident radiation. In figure 31 a further angle i_1', is used to indicate the complete masking of the groove from the incident radiation for

FIGURE 31. Measured variation of zero and first order ($m = +1$) diffraction efficiencies with incidence angle at 0.154 nm, for a groove depth of 11 nm.

FIGURE 32. Calculated variation of zero and first order ($m = +1$) diffraction efficiencies with incidence angle at 0.154 nm, for various groove depths h. Partial masking model.

534   A. FRANKS AND OTHERS

Figure 33. (a) Measured variation of zero and first order ($m = +1$) diffraction efficiencies with incidence angle at 0.154 nm, for a groove depth of 18 nm. (b) Calculated variation of zero order diffraction efficiencies with incidence angle at 0.154 nm, for various groove depths h. Partial masking model. (c) Calculated variation of first order ($m = +1$) diffraction efficiencies with incidence angle at 0.154 nm, for various groove depths h. Partial masking model.

a groove depth $h = 7$ nm approximately, where the latter groove depth was that determined for grating no. 78 (gold coated) in the analysis, described above, of the performance curves at $\lambda = 0.83$ nm.

It is clear from the figures 29 and 30 that over the majority of the range of grazing incidence angles, the grooves are illuminated directly by the incident beam, while in figure 31 this is true only over the latter half of the range. For a comparison of the experimental performance with theory, a number of predicted performance curves at various groove depths are plotted in figure 32. (The theory is based on a model with equal land and groove widths, the applicability of which is discussed later.) The peak which occurs at $i \approx 22'$ for $h \approx 3$ nm (figure 32), corresponds to the primary maximum of efficiency in the first order.

There appears to be reasonable qualitative agreement between the experimental and theoretical curves, provided allowance is made for the shadowing effects where the land-to-groove width ratio is not unity (as was the case for the gratings investigated. The results obtained are as follows

(i) For very shallow grooves ($h \approx 2$ nm), the predicted performance shown in figure 32 is relatively flat and this corresponds reasonably well with the first order performance of grating no. 76 (figure 29).

(ii) In the case of grating no. 77, assuming a true groove depth of about 5 nm (estimated groove depth is 6.5 nm), the experimental performance curve would be expected to fall off prematurely for decreasing i, compared with the theoretical curve, as a result of the proportionally larger shadowing effects in the grooves, since the land width was approximately 1.5 times that of the groove. Also at shallow angles $i < 10'$, where $i_1 = 10'$ for $h = 5$ nm, much of the radiation incident in the groove regions will be absorbed by the grating material, since it cannot illuminate the next groove by penetration through the material barrier over an appreciable angular range, owing to the fact that the land-to-groove width ratio is not unity. Thus it might well be anticipated that the major contribution to the diffracted energy at $i < 10'$ would come from the land areas, while a significant contribution would arise from the grooves at $i > 10'-15'$. This would explain the gradual increase in performance for increasing i.

(iii) The performance curve of grating no. 78 shown in figure 31, shows a marked similarity to the predicted performance at $h \approx 10$ nm, at angles where $i > 16'$. The fact that there is little correlation of experiment with theory below this angle and none for $i < 10'$, where an increase in performance is expected from the predicted results, might well be explained again by the fact that the land areas were wider than the grooves by a factor of 1.2. Thus much of the radiation at shallow angles was lost by absorption in the grating material as a result of the proportionally large masking effects, together with the fact that the next and subsequent grooves were not illuminated by the incident radiation over a range of incidence angles (as in (ii) above).

The zero and first order performance curves of grating no. 83 are shown in figure 33a. Here the oscillatory nature of both orders is clearly visible. The first order ($m = +1$) oscillations are analysed in relation to figure 34, which is a logarithmic plot of h against i for the location of stationary points defined by the integer n on the oscillatory performance curves. For a groove depth of $h = 15$ nm it is clear that the minimum at $i = 25'$, corresponds to $n = 4$, but it is slightly displaced in the direction of decreasing i as a result of the fall-off in reflectivity at such large angles. The first maximum at $i = 17'$ corresponds to $n = 3$ and the second maximum

55

at $i = 29'$ to $n = 5$. The maximum corresponding to $n = 5$ would occur at $i = 37'$, but the peak is cut off prematurely by the sharp reflexion cut-off at $i \approx 30'$ for $\lambda = 0.154$ nm.

In this analysis, no account has been taken of the fact that the radiation which penetrates the material barriers supporting the lands traverses an optical path length shorter than that which would be traversed *in vacuo*, since the refractive index is slightly less than unity. The effect of this difference in path length on the uncorrected maxima and minima would be for these to correspond to a slightly shallower groove depth. The path difference introduced on entering the groove is given by $z = 2h \sin i$ (in the zero order). Hence $\delta z = 2\delta h \sin i$. Now in the present case (grating no. 83), the difference between the optical path through 1.35μm of material and vacuum is approximately 0.05 nm. Thus at $i = 24'$, this corresponds to a groove depth change $\delta h = 3$ nm approximately. The effect of this optical path difference introduced as a result of penetration is to displace the stationary points in the direction of increasing i, in figure 34, and thus indicate an apparently shallower groove.
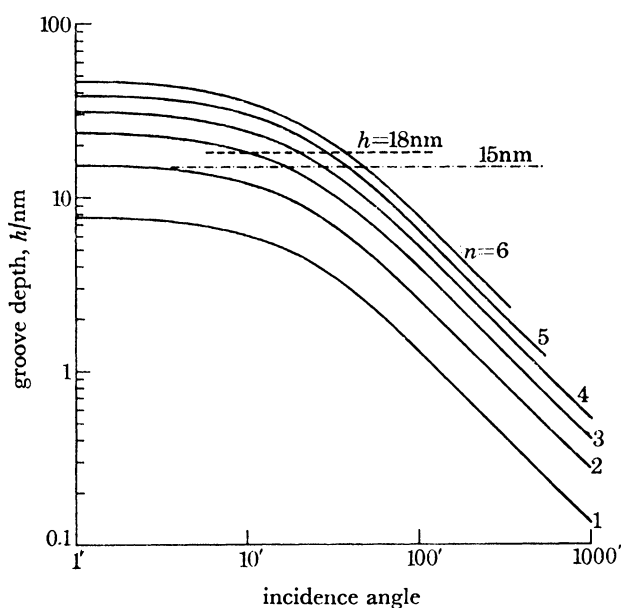
FIGURE 34. Relation between groove depth and incidence angle for the first three maxima and minima ($n = 1$–6) in the first spectral order ($m = +1$) for 300 lines/mm gratings, at 0.154 nm.

In the theoretically predicted performance curves, for both the zero and first orders, this optical path difference is taken into consideration, and is here applied to a land-to-groove width ratio of unity. The theoretical curves are shown in figures 33b, c for a range of groove depths of 14–18 nm. Good qualitative agreement is found between theory and experiment for grating no. 83 at $h = 16$ nm for the zero order for $i > 16'$ and at $h = 17$ nm for the first order for $i > 12'$. The oscillations at $i = 8'$ in both the zero and first order predicted curves are due to the illumination of different grooves (denoted by integer p in figure 9) as a result of the penetration of the incident radiation through the grating material, as the grazing incidence angle i decreases.

The predicted curves do not fit the experimental curves for shallow angles $i < 12'$ in the first order and $i < 16'$ in the zero order. In the case of the first order, this may be partly

explained by accepting an 'averaged' predicted curve from those shown in figure 33 c, where the groove undulations may be about ± 2 nm. A relatively smooth curve would result.

The oscillations observed at shallow angles of grazing incidence in the zero order curves of the gratings discussed so far and also to be seen in grating no. 87 later, are possibly due to two effects

(i) the illumination of different grooves, related to the integer p, as a result of penetration of the incident beam through the material barriers under the land areas. These oscillations are predicted in figure 33 b and are not smoothed out on taking an 'averaged' curve of those shown, unlike the case for the first order in figure 33 c, since the oscillations are roughly in phase along the incidence angle axis and

(ii) the interface between those fractions of radiation reflected from the vacuum-gold interface and the gold-substrate interface, similar to Kiessig interference patterns, which occur near the critical angle of reflexion. Similar observations have, however, been observed in uncoated Spectrosil gratings and this lends weight to the assumption in (i).
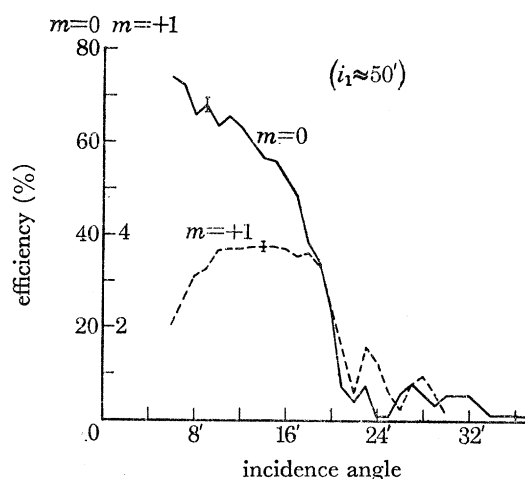
FIGURE 35. Measured variation of zero and first order ($m = +1$) diffraction efficiences with incidence angle at 0.154 nm, for a groove depth of 35 nm.

This interpretation is further confirmed by the tests on grating no. 87, where the grooves were too deep to be directly illuminated for incidence angles up to 40' ($i_1 = 50'$ for $h = 35$ nm and $i_1 = 40'$ for $h = 30$ nm for this grating). The zero and first orders are shown in figure 35 where the oscillatory nature of the curve, particularly for $i > 20'$, shows without doubt that the grooves are contributing to the diffracted energy at these shallow angles. The theoretical efficiency curve was extremely sensitive to variations in h and i because of the relatively large groove depths and wavelenths used, and thus a rough correlation only between theory and experiment was possible.

(c) *Effect of coating thickness, performance at short wavelengths, short wavelength cut-off and resolving power*

In this section, aspects other than phase grating behaviour are discussed.

Nearly one hundred gratings have been examined in the short wavelength region (0.05–0.5 nm) often by using both photographic film (Franks & Lindsey 1968) and proportional

counters. The photographic technique is particularly useful for obtaining a rapid survey of grating performance and assessing grating perfection. Structure in the spectral lines arising from grating surface defects is easily observed and interpreted by photographic methods.

(i) Coating thickness

The principal effect of gold coating a Spectrosil mirror is to enhance reflexion efficiency at angles exceeding the critical glancing angle for silica and this is illustrated in figure 36 for different thicknesses of gold. Reflexion efficiency is not, however, the only criterion which must be taken into account. Surface perfection gradually diminishes as the thickness increases, thus giving rise to increased scatter and ultimately this must also lead to a decrease in reflectivity. In general, the reflectivity curve gradually transforms from that of the substrate to that of the coating, as the thickness increases (Parratt 1954). In the case of a grating, the increase and subsequent decrease in diffraction efficiency as the gold thickness increases is shown in figure 37.

At short wavelengths, where penetration of the material barriers supporting the lands takes place, an additional factor must be taken into account. Figure 38 illustrates a Spectrosil grating
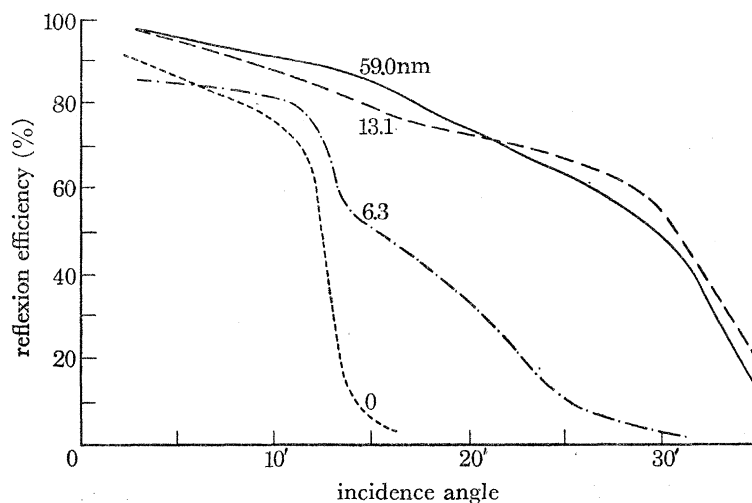
FIGURE 36. Measured variation of reflexion efficiency with incidence angle at 0.154 nm, for various gold thicknesses on a Spectrosil mirror.
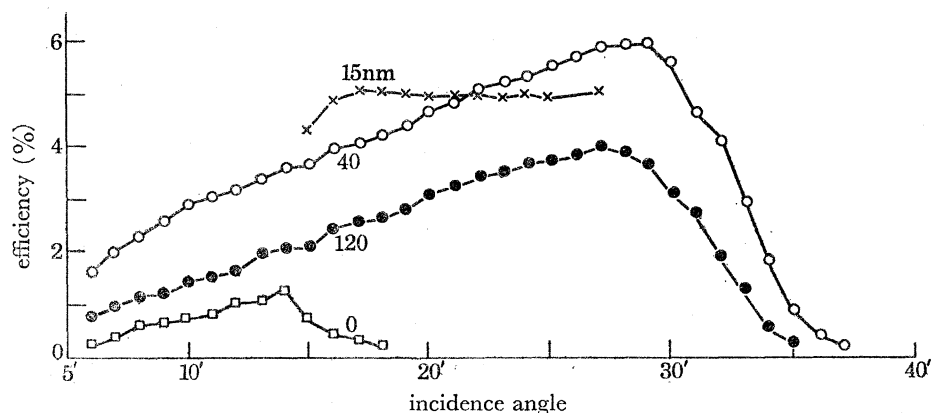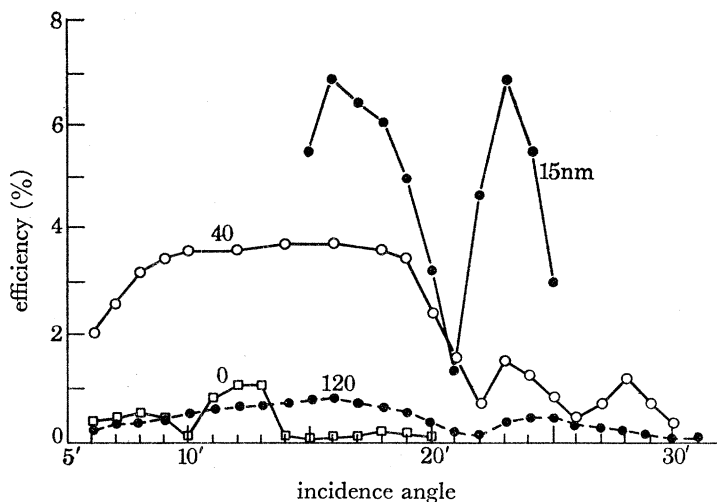

FIGURE 37. Measured variation of first order $(m = +1)$ diffraction efficiencies with incidence angle at 0.154 nm, for various gold thicknesses on a grating with a groove depth of 7 nm.

coated with a thin layer of gold, where the thickness of the layer is small compared with the groove depth. The ray shown penetrates the barrier supporting the land BC. It is diffracted from the gold surface of groove CD and penetrates the barrier supporting the land DE and then escapes from the grating surface to contribute to the diffraction image. If the gold coating thickness were greater than the groove depth, then the ray would pass through gold barriers BC and DE, where the absorption would be high. For example, at a wavelength of 0.154 nm, the intensity of the transmitted beam is reduced by $1/e$ in a distance of approximately 2.5 μm for gold and 95 μm for silica. This model is completely consistent with the experimental results in that higher efficiencies were obtained where the groove depth exceeded the coating thickness. Figure 39 illustrates the variation in first order diffraction efficiencies for various gold thicknesses and the decrease in intensity and modulation when the coating thickness exceeds the groove depth.
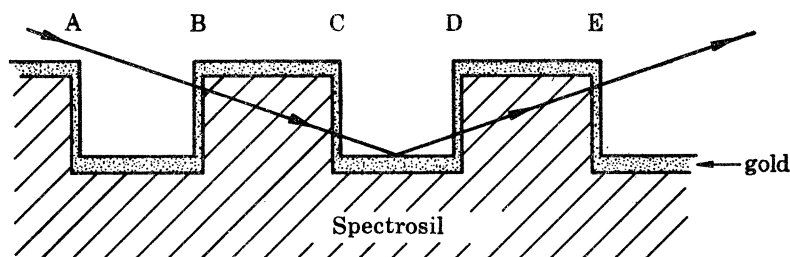
FIGURE 38. Effect of gold coating a grating.

FIGURE 39. Measured variation of first order ($m = +1$) diffraction efficiencies with incidence angle at 0.154 nm, for various gold thicknesses on a grating with a groove depth of 40 nm.

Both figures 37 and 39 also illustrate an important experimental result which is invariably obtained, but for which no satisfactory explanation is as yet forthcoming. It is found that the diffraction efficiency with no coating, at all the wavelengths investigated, is always considerably less than that of a gold coated grating, even at small grazing angles where the reflectivities of a coated and uncoated mirror (figure 36) do not differ by more than about 15%.

(ii) *Performance at wavelengths below* 0.1 nm

This effect is also shown for grating no. 87 at even shorter wavelengths (Ag K radiation, $\lambda = 0.056$ nm), in figure 40. It is of interest to note that the maximum first order diffraction efficiency obtained is slightly over 0.5 % and this is an order of magnitude smaller than the corresponding efficiency at 0.154 nm. This leads us to speculate whether there is a short wavelength limit below which grating efficiency becomes impracticably small.
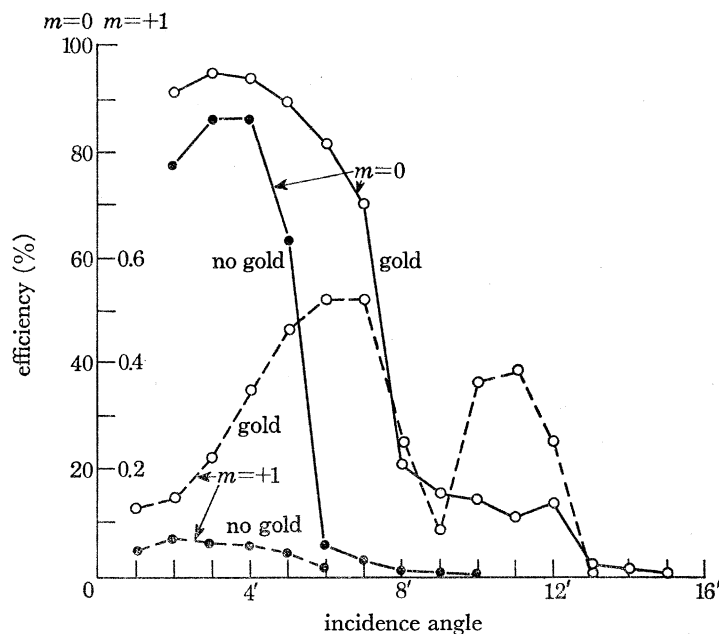

FIGURE 40. Measured variation of zero and first order $(m = +1)$ diffraction efficiencies with incidence angle at 0.056 nm, both with the grating uncoated and coated with 40 nm of gold.

The path difference arising from an imperfection of height H on the surface in the direction of the diffracted beam is $H(\sin i + \sin \theta)$. In a peak efficiency position in the first order (figure 40), $i = 12'$ and $\theta = 23'$. Hence for a path difference of $\frac{1}{2}\lambda$, the height of the imperfection is 2.8 nm. For aberration or scatter free performance the imperfections must be a small fraction of this amount and thus approach atomic dimensions. In fact, the surface perfection achieved is about 1 nm so that in this particular case there is a small factor in hand. This argument does however lead to the conclusion that there is a short wavelength limit below which it is unlikely that useful diffraction efficiency can be obtained – the incoherent scatter becoming predominant as the diffraction efficiency tends to zero – and that this wavelength limit is in the region of 0.01–0.04 nm. It should be possible to extend the limit to somewhat shorter wavelengths by increasing the grating spacing and thus decreasing the value of θ. There is, however, also a limitation on this procedure since the diffraction angles then become too small to be measured conveniently.

(iii) *Short wavelength cut-off*

At any given incidence angle, the short wavelength cut-off for the zero order occurs when the transmitted (refracted) radiation is parallel to the grating surface. Taking the Wood's anomaly argument further, Miller (1964) has shown that all orders diffracted at angles larger than the

zero order are similarly cut-off when the corresponding transmitted orders are parallel to the grating surface. Fujiwara & Iguchi (1968) reached an identical conclusion and confirmed this by measurements in the visible region of the spectrum.

By using the theory due to Hönl (1933) to derive the refractive index of gold, the critical angle is found to be 20′ at 0.095 nm and 10′ at 0.0422 nm. The wavelength cut-off of the continuum spectrum is shown in figure 41, plate 18, and was obtained with grating no. 71 by using the 5 m A.W.R.E. spectrograph. At a 20′ incidence angle the measured cut-off was 0.093 ± 0.001 nm. The figure also illustrates the decrease in cut-off wavelength with decreasing incidence angle.

At 10′ the cut-off was not so clearly visible because of scattered radiation. When this was reduced by obscuring the zero order with a knife edge, a cut-off was observed at 0.051 ± 0.001 nm. By using a fluorescent X-ray source, the $K\alpha$ line of indium (0.0514 nm) was recorded, but not the Sn $K\alpha$ line (0.0491 nm).

(iv) *Resolving power*

There is no reason to suppose that the grating manufacturing processes employed would in any way cause a loss of resolving power. The predominant factor which determines resolving power under small incidence angle conditions is the source size or entrance slit width. This is illustrated in figure 42 obtained with the spectrograph and which shows the first order diffraction line width as a function of entrance slit width at a wavelength of 0.166 nm (Ni $K\alpha$ radiation). The experimental results coincide within the limits of experimental error with the theoretical line width $\delta\lambda = dw/R$, where d is the grating spacing, w is the slit width and R the grating radius.
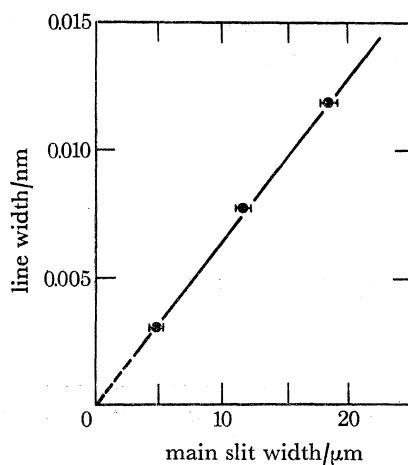

FIGURE 42. Line width at half height as a function of main slit width for Ni $K\alpha$ radiation (0.166 nm).

Figure 43, plate 19, shows the spectrum obtained with a tungsten target at an incidence angle of 20′ and with a 2 μm wide entrance slit. The $L\alpha_1$ and $L\alpha_2$ radiations, differing in wavelength by 0.0011 nm, are resolved on the original plate. The theoretical resolving power for this slit width is 0.0013 nm.

7. SUMMARY AND DISCUSSION

The relations between diffraction efficiency, wavelength, incidence angle and groove depth in a phase grating can be accounted for reasonably well, qualitatively, by means of scalar theory. It should thus be possible to design a grating to have an optimum performance in any selected region of the spectrum.

No theory has been found which is capable of determining the absolute values of diffraction efficiency.

Measured values of first order diffraction efficiencies range from 20 % in the 1 nm region to between 5 and 10 % in the 0.1–1 nm range and below 1 % at wavelengths less than 0.1 nm, where the incidence angles are about 5′. The limitation on diffraction efficiency at very short wavelengths may arise from roughness, on an atomic scale, of the diffracting surface.

REFERENCES

Bennett, J. M. 1969 *J. Phys.* E **2**, 816–817.
Bennett, J. M. 1971 Physical structure and diffraction performance of laminar X-ray gratings. Ph.D. Thesis, The University of London.
Blodgett, K. B. 1935 *J. Am. chem. Soc.* **57**, 1007–1022.
Butler, D. W. 1973 *Micron.* **4**, 410–424.
Franks, A. & Lindsey, K. 1966 *The electron microprobe. Electron probe microanalysis of the low atomic number element with N.P.L. X-ray gratings* (ed. T. D. McKinley, K. F. J. Heinrich & D. B. Wittry), pp. 83–92. New York: J. Wiley.
Franks, A. & Lindsey, K. 1968 *J. Phys.* E **1**, 144.
Fujiwara, S. & Iguchi, Y. 1968 *J. opt. Soc. Am.* **58**, 361–367 and 1189–1191.
Hönl, H. 1933 *Ann. Phys.* **18**, 625–655.
Hellwege, K. H. 1937 *Z. Phys.* **106**, 588–596.
Kiessig, H. 1931 *Ann. Phys.* **10**, 769–788.
Lindsey, K. 1973 *Proc. Conf. on X-ray Optics in Astronomy* (ed. P. W. Sanford), pp. 101–121. The University of London: Mullard Space Science Laboratory.
Miller, J. C. 1964 *J. opt. Soc. Am.* **54**, 353–356.
Palmer, C. H. 1952 *J. opt. Soc. Am.* **42**, 269–276.
Palmer, C. H. 1956 *J. opt. Soc. Am.* **46**, 50–53.
Parratt, L. G. 1954 *Phys. Rev.* **95**, 359–369.
Sayce, L. A. & Franks, A. 1964 *Proc. R. Soc. Lond.* A **282**, 353–357.
Speer, R. J. 1966 An extreme ultraviolet monochromator for solar studies. Ph.D. Thesis, The University of London.
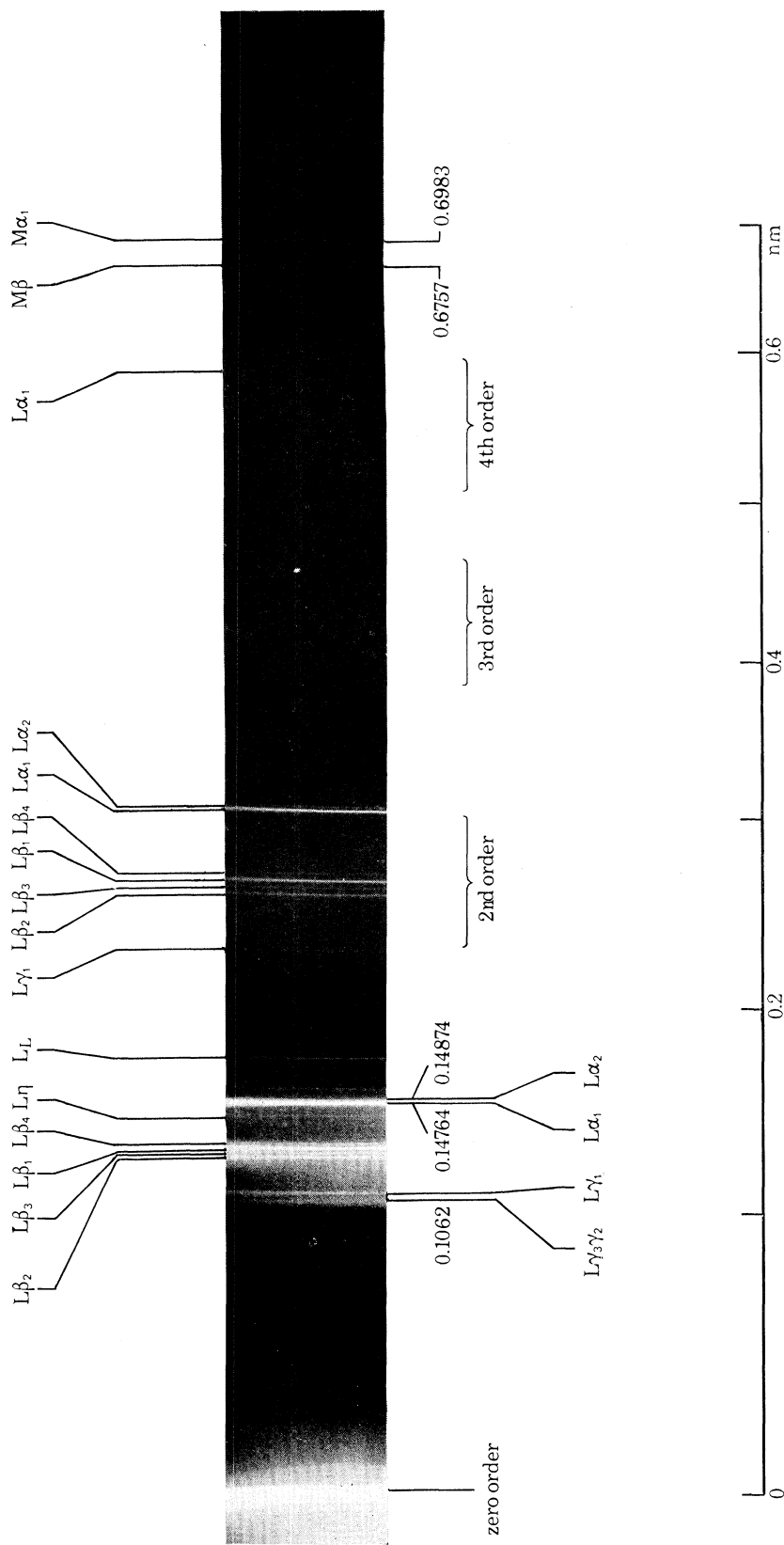Speer, R. J. 1970 *Adv. X-ray Analysis* **13**, 382–389.

Franks et. al.

Phil. Trans. R. Soc. Lond. A, volume 277, *plate* 19

FIGURE 43. L and M spectra of tungsten. Incidence angle is 20′.

Speer, R. J. 1972 *Atoms and molecules in astrophysis* (ed. T. R. Carson & M. J. Roberts), pp. 285–309. London: Academic Press.

Speer, R. J. & Turner, D. 1973 *Proc. Int. Symp. for Synchrotron Radiation Users*, 106–114. Daresbury Nuclear Physics Laboratory Report no. 26.

Speer, R. J., Peacock, N. J., Waller, W. A. & Osborne, P. J. 1970 *J. Phys.* E **3**, 143–147.

Stanley, V. W., Franks, A. & Lindsey, K. 1968 *J. Phys.* E **1**, 643–645.

Stewardson, E. A. & Underwood, J. H. 1965 *Brit. J. app. Phys.* **16**, 1877–1884.

Verrill, J. 1973 *J. Phys.* E **6**, 1199–1201.

Wood, R. W. 1902 *Phil. Mag.* **4**, 396–402.

Wood, R. W. 1912 *Phil. Mag.* **23**, 315–317.

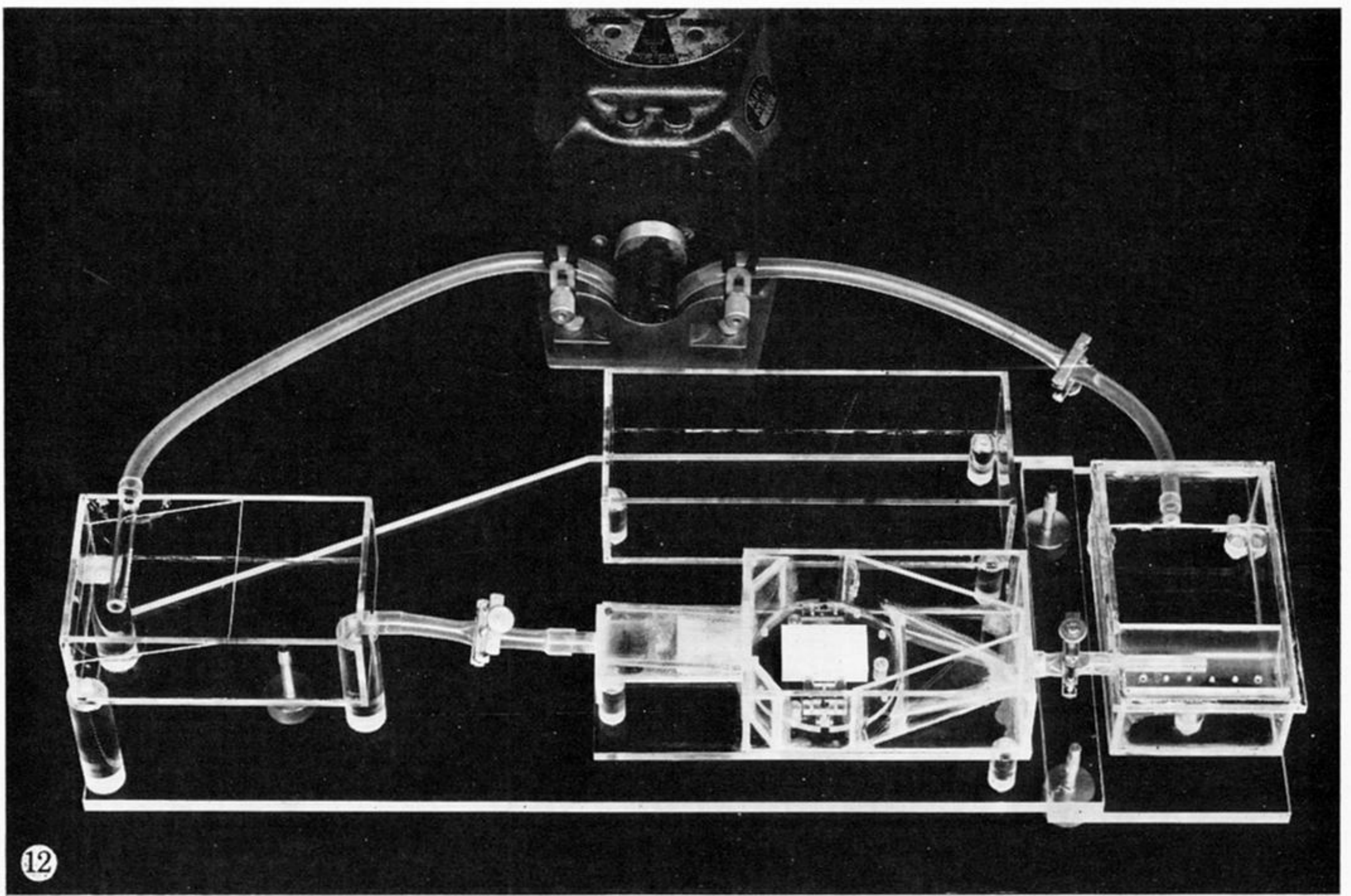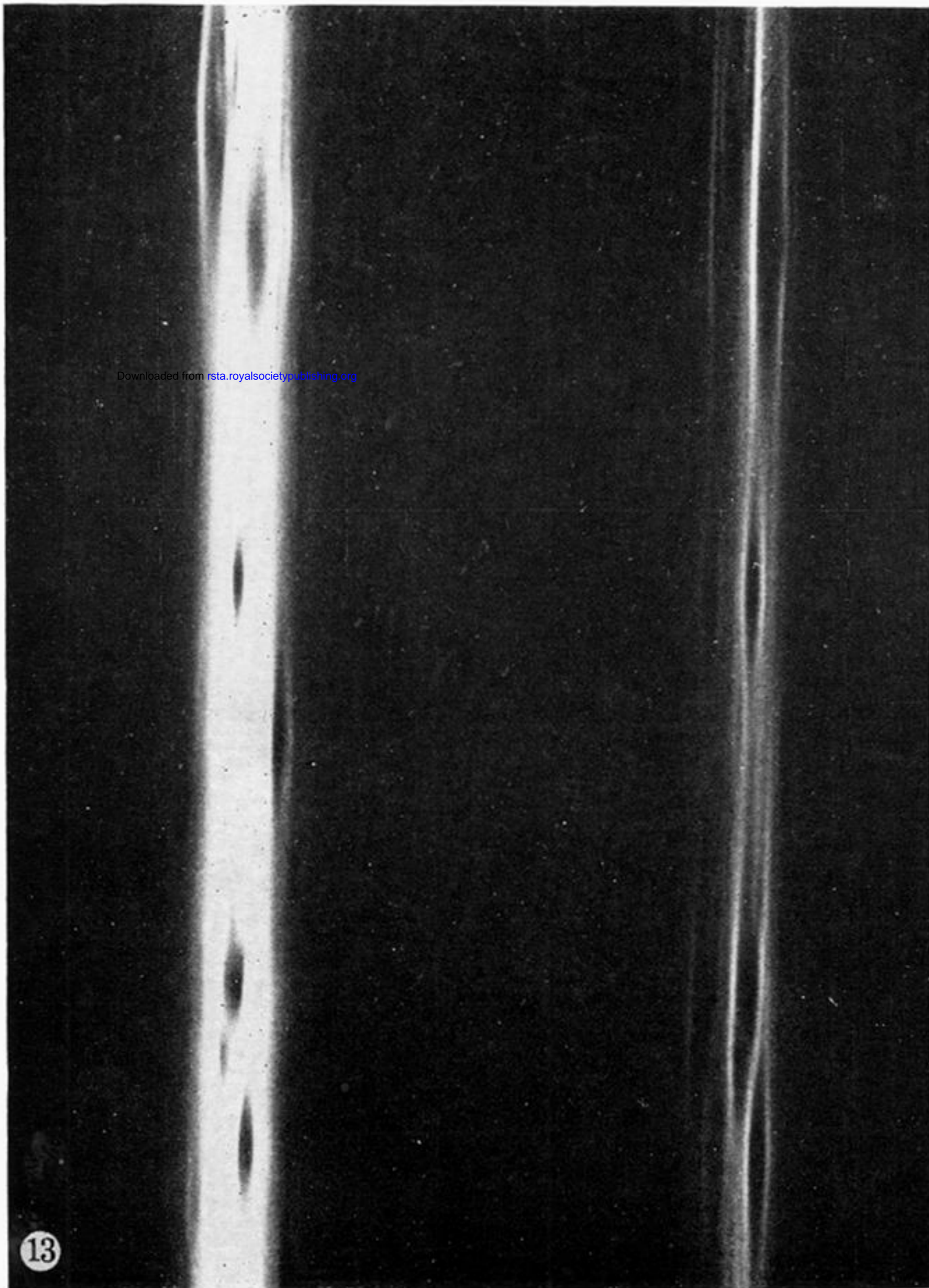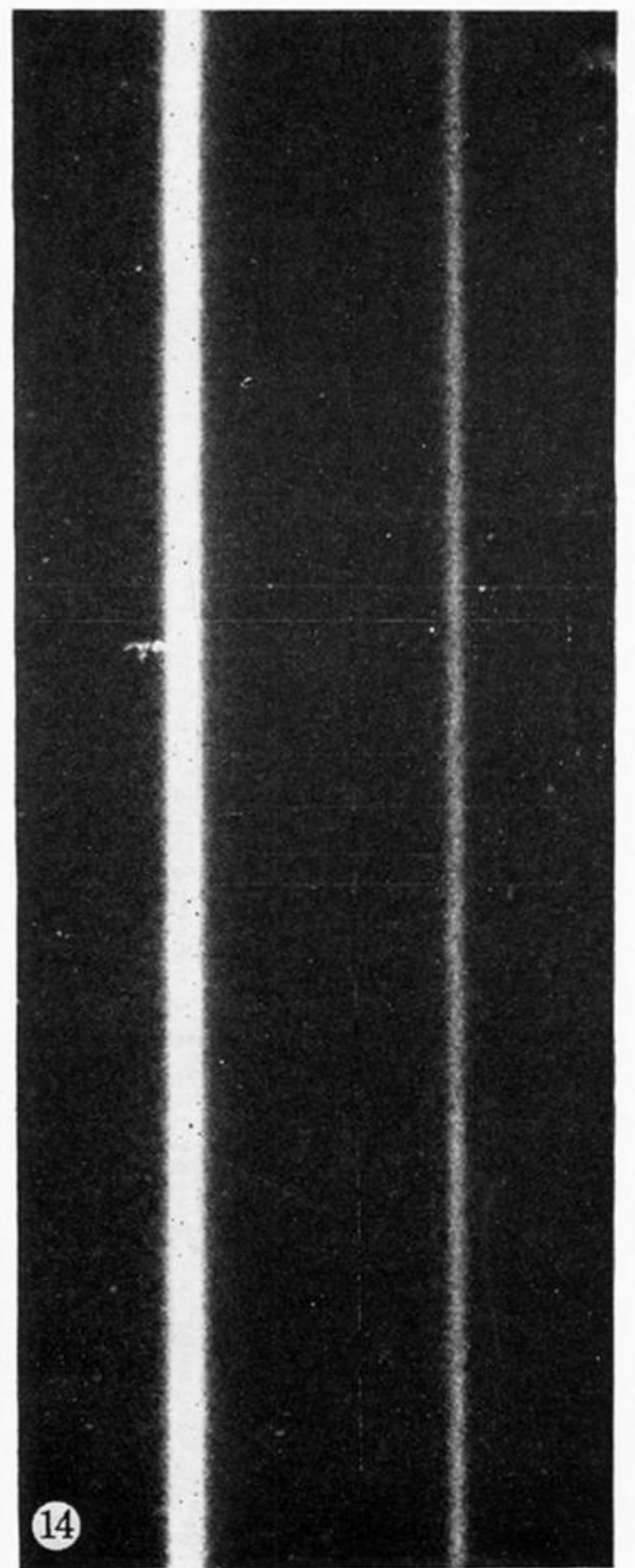Wood, R. W. 1935 *Phys. Rev.* **48**, 928–936.

FIGURE 2. Electron micrograph of N.P.L. X-ray phase grating (300 lines/mm) illustrating the laminar configuration (the fine surface structure is produced by the electron microscope replica technique employed).
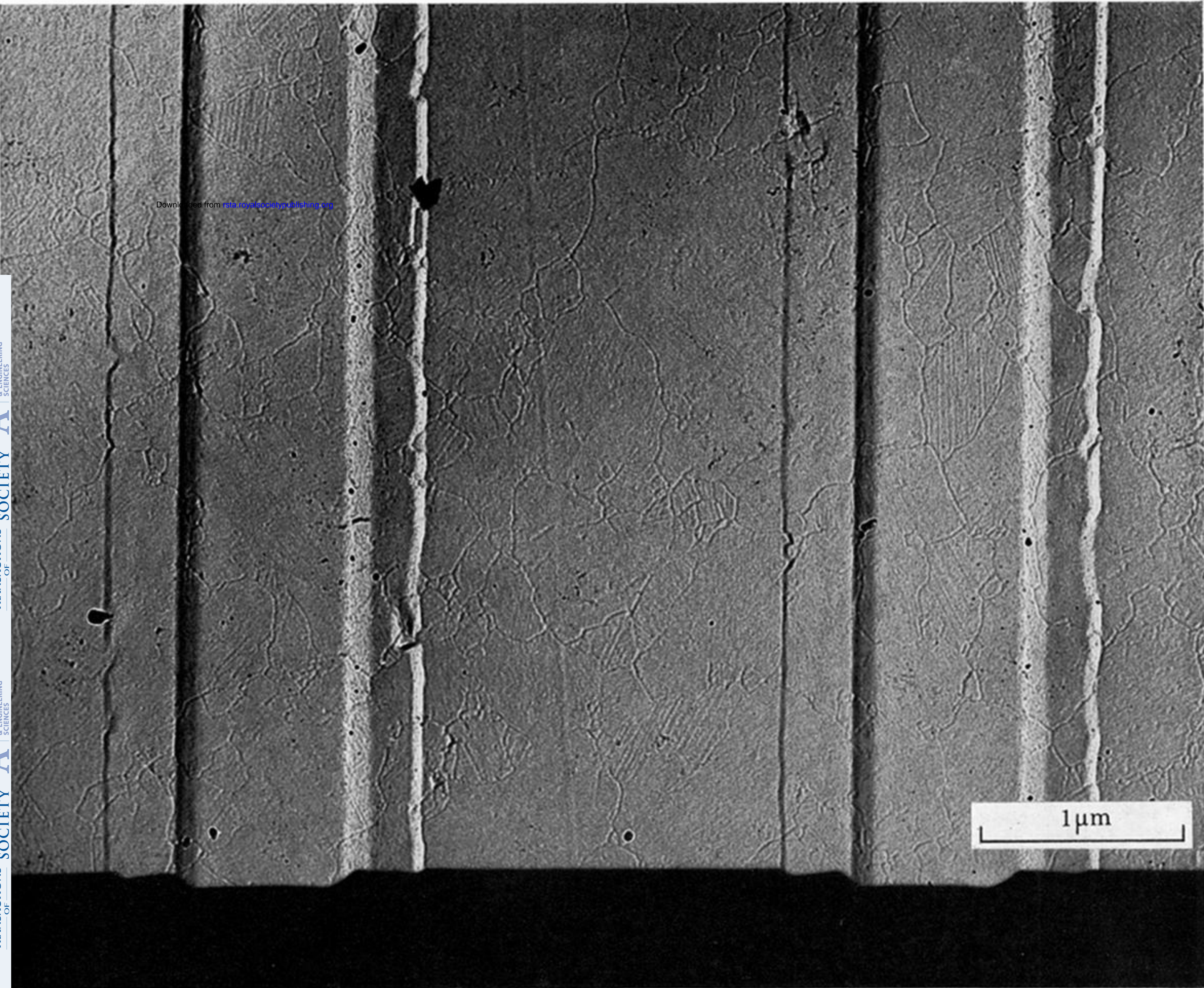
Figure 12. The perspex chemical etching assembly showing a grating in position in the etching bath (centre).

Figure 13. Structure at secondary foci in the zero and first order spectra obtained with an imperfect 5 m concave grating. ($\lambda = 0.154$ nm.)

Figure 14. Zero and first order spectra from a structure-free 5 m concave grating. ($\lambda = 0.154$ nm.)

FIGURE 15. Montage showing electron micrograph of a 300 lines/mm grating surface and profile.

FIGURE 41. Dependence of first order short wavelength cut-off on incidence angle.

$L\beta_2$ $L\beta_3$ $L\beta_1$ $L\beta_4$ $L\eta$ L_L $L\gamma_1$ $L\beta_2$ $L\beta_3$ $L\beta_1$ $L\beta_4$ $L\alpha_1$ $L\alpha_2$ $L\alpha_1$ $M\beta$ $M\alpha_1$

0.1062 0.14764 0.14874 0.6757 0.6983

zero order

2nd order   3rd order   4th order

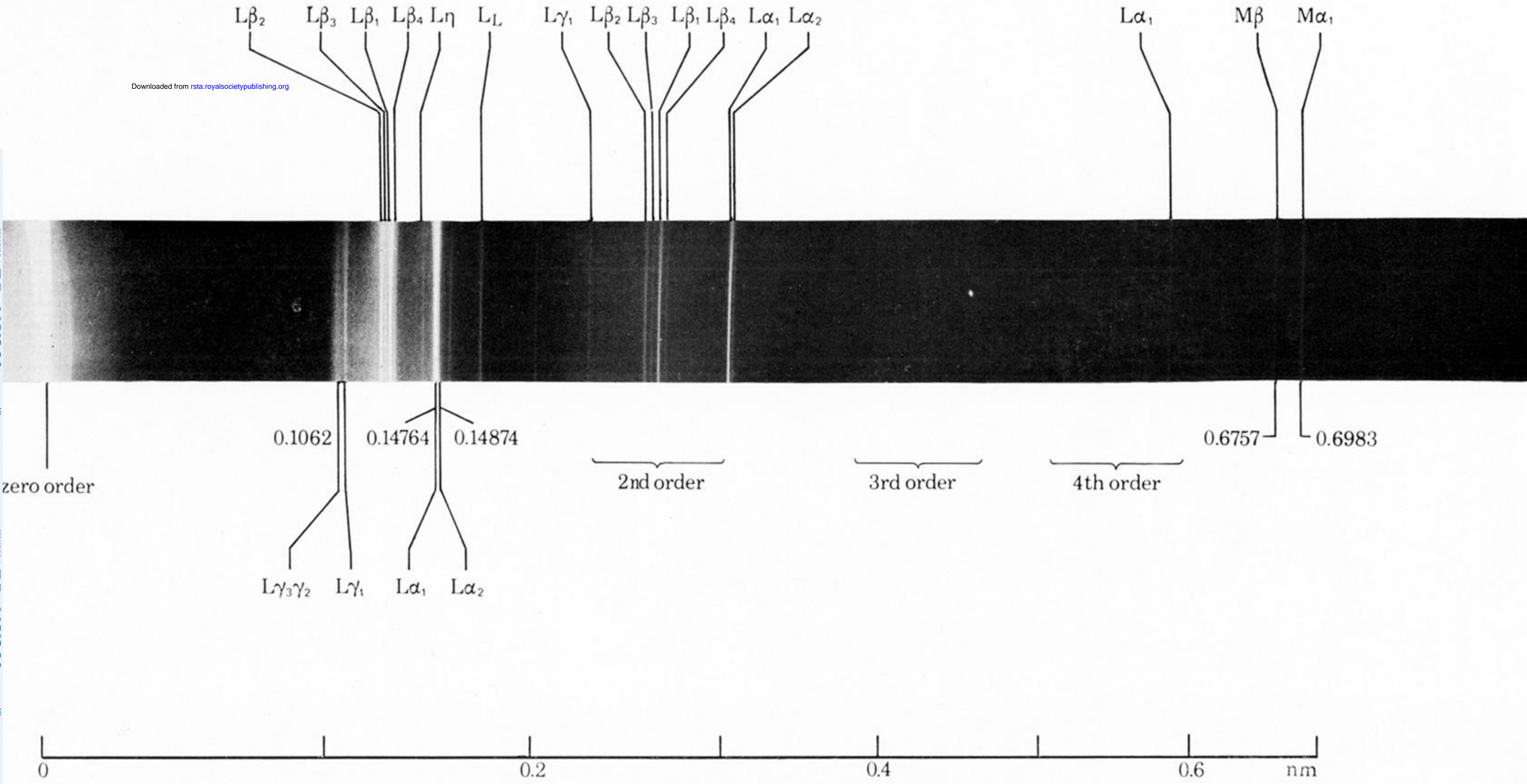$L\gamma_3\gamma_2$ $L\gamma_1$ $L\alpha_1$ $L\alpha_2$

0   0.2   0.4   0.6   nm

FIGURE 43. L and M spectra of tungsten. Incidence angle is 20′.